ATLAS NOTE

ATLAS-CONF-2013-082

August 8, 2013

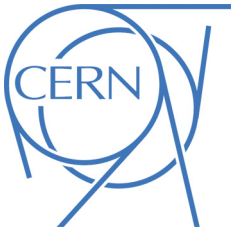

Performance of Missing Transverse Momentum Reconstruction in ATLAS studied in Proton-Proton Collisions recorded in 2012 at $\sqrt{s}$ = 8 TeV

ATLAS Collaboration

Abstract

The performance of the missing transverse momentum reconstruction in the ATLAS detector is evaluated using data collected in 2012 in proton-proton collisions at a centre-of-mass energy of 8 TeV. An optimised reconstruction and calibration of the missing transverse momentum is used and the effects arising from additional proton-proton interactions superimposed on the hard physics process are suppressed with various methods. Results are shown for a data sample corresponding to an integrated luminosity of about 20 fb^{-1} and for events with different topologies with or without genuine missing transverse momentum due to undetected particles. Estimates of the systematic uncertainty on the missing transverse momentum measurement are also presented.

ATLAS-CONF-2013-082
09 August 2013

1 Introduction

In a hadron collider event the missing transverse momentum is defined as the momentum imbalance in the plane transverse to the beam axis, where momentum conservation is useful. Such an imbalance may signal the presence of undetectable particles, such as neutrinos or new weakly-interacting particles. The vector momentum imbalance in the transverse plane is obtained from the negative vector sum of the momenta of all particles detected in a proton-proton (pp) collision and is denoted as missing transverse momentum, $\boldsymbol{E}_{\mathrm{T}}^{\mathrm{miss}}$. The symbol $E_{\mathrm{T}}^{\mathrm{miss}}$ is used for its magnitude.

An optimised reconstruction and calibration of $\boldsymbol{E}_{\mathrm{T}}^{\mathrm{miss}}$ [1] was developed by the ATLAS Collaboration. The $\boldsymbol{E}_{\mathrm{T}}^{\mathrm{miss}}$ measurement is significantly affected by the contributions of additional pp collisions superimposed on the hard physics process, referred to as pile-up in the following, so methods were developed to suppress such contributions [2]. This note describes the performance, in terms of resolution, response and tails, of the reconstructed $\boldsymbol{E}_{\mathrm{T}}^{\mathrm{miss}}$ after pile-up suppression.

The event samples used to assess the quality of the $\boldsymbol{E}_{\mathrm{T}}^{\mathrm{miss}}$ reconstruction are minimum bias events, events with leptonically decaying W and Z bosons and simulated events with large jet multiplicity and/or large missing transverse momentum, such as $H \to \tau\tau$, $t\bar{t}$ and simulated supersymmetric (SUSY) events. These test the detector capability in the reconstruction and calibration of different physics objects, the optimization of the $\boldsymbol{E}_{\mathrm{T}}^{\mathrm{miss}}$ calculation and the methods of pile-up suppression. The $\boldsymbol{E}_{\mathrm{T}}^{\mathrm{miss}}$ performance is studied in both data and Monte Carlo simulation and comparisons are made. The study of $\boldsymbol{E}_{\mathrm{T}}^{\mathrm{miss}}$ performance in events where genuine $E_{\mathrm{T}}^{\mathrm{miss}}$ is present allows for a validation of the $E_{\mathrm{T}}^{\mathrm{miss}}$ scale. In simulated events, the genuine $E_{\mathrm{T}}^{\mathrm{miss}}$ is calculated from all non-interacting particles in the event, including neutrinos from heavy flavour decay, and is referred to as true $E_{\mathrm{T}}^{\mathrm{miss}}$ ($E_{\mathrm{T}}^{\mathrm{miss,True}}$) in the following.

An important requirement on the measurement of $\boldsymbol{E}_{\mathrm{T}}^{\mathrm{miss}}$ is maximizing detector coverage and reducing the effect of finite detector resolution, the presence of dead regions and different sources of noise, as well as cosmic-ray and beam-halo muons crossing the detector, that can produce fake $E_{\mathrm{T}}^{\mathrm{miss}}$. The ATLAS calorimeter coverage extends to large pseudorapidities[1] to reduce the impact of high energy particles escaping in the very forward direction. However, there are transition regions between different calorimeters containing inactive material which lead to increased fake $E_{\mathrm{T}}^{\mathrm{miss}}$. Selection criteria are applied to reduce the impact of these sources of fake $E_{\mathrm{T}}^{\mathrm{miss}}$.

This note is organised as follows. Section 2 gives a brief introduction to the ATLAS detector. Sections 3 and 4 describe the data and Monte Carlo samples used and the event selections applied. Section 5 outlines how $\boldsymbol{E}_{\mathrm{T}}^{\mathrm{miss}}$ is reconstructed and calibrated and Section 6 summarizes the methods used to mitigate the pile-up effects. Section 7 presents the $\boldsymbol{E}_{\mathrm{T}}^{\mathrm{miss}}$ performance for data and Monte Carlo simulation in events from different physics channels with various topologies. Finally, the systematic uncertainty on the $E_{\mathrm{T}}^{\mathrm{miss}}$ absolute scale is discussed in Section 8.

2 The ATLAS Detector

The ATLAS detector [3] is a multipurpose particle physics apparatus with a forward-backward symmetric cylindrical geometry and near 4π coverage in solid angle. The inner tracking detector (ID) covers the pseudorapidity range $|\eta| < 2.5$, and consists of a silicon pixel detector, a silicon microstrip detector (SCT), and, for $|\eta| < 2.0$, a transition radiation tracker (TRT). The ID is surrounded by a thin superconducting solenoid providing a 2 T magnetic field. A high-granularity lead/liquid-argon (LAr) sampling electromagnetic calorimeter covers the region $|\eta| < 3.2$. A steel/scintillator-tile calorimeter provides

[1] ATLAS uses a right-handed coordinate system with its origin at the nominal interaction point (IP) in the centre of the detector and the z-axis coinciding with the axis of the beam pipe. The x-axis points from the IP to the centre of the LHC ring, and the y axis points upward. Cylindrical coordinates (r, ϕ) are used in the transverse plane, ϕ being the azimuthal angle around the beam pipe. The pseudorapidity is defined in terms of the polar angle θ as $\eta = -\ln\tan(\theta/2)$.

hadronic coverage in the range $|\eta| < 1.7$. LAr technology is also used for the hadronic calorimeters in the end-cap region $1.5 < |\eta| < 3.2$ and for both electromagnetic and hadronic measurements in the forward region up to $|\eta| < 4.9$. The muon spectrometer surrounds the calorimeters. It consists of three large air-core superconducting toroid systems, precision tracking chambers providing accurate muon tracking out to $|\eta| = 2.7$, and additional detectors for triggering in the region $|\eta| < 2.4$.

3 Data samples and event selection

During 2012, proton-proton (pp) collisions at a centre-of-mass energy of 8 TeV were recorded with stable proton beams and nominal ATLAS magnetic field conditions. Only data with a fully functioning calorimeter, inner detector and muon spectrometer are analysed.

Selection criteria [4] are applied which reduce the impact of instrumental noise and out-of-time energy deposits in the calorimeter from cosmic-rays or beam-induced background, suppressing the effect of fake $E_{\mathrm{T}}^{\mathrm{miss}}$ from those sources.

The data sets used correspond to a total integrated luminosity [5, 6] of approximately $20\,\mathrm{fb}^{-1}$, collected in 2012 with a bunch crossing interval (bunch spacing) of 50 ns. The mean number of interactions per bunch crossing ($\langle\mu\rangle$)[2] was about 20.7, with $\langle\mu\rangle$ reaching values up to 35 at the beginning of a fill during the 2012 LHC running period.

Trigger and selection criteria applied for the study of minimum bias events and events with leptonically decaying W and Z bosons are described in the following.

3.1 Minimum bias events

Minimum bias events were selected both by a random trigger and by the minimum bias trigger scintillators (MBTS), which are mounted at each end of the detector in front of the LAr end-cap calorimeter cryostats [7]. For each event, at least one good primary vertex is required with a z displacement from the nominal pp interaction point of less than 200 mm and with at least five associated tracks.

3.2 $Z \to \ell\ell$ event selection

Candidate $Z \to \ell\ell$ events, where ℓ is an electron or a muon, are required to pass an electron, photon or muon trigger with a transverse momentum, p_{T}, threshold between 15 and 20 GeV, where the exact trigger selection varies depending on the data period analysed. For each event, at least one good primary vertex is required with a z displacement from the nominal pp interaction point of less than 200 mm and with at least three associated tracks.

The selection of $Z \to \mu\mu$ events requires the presence of exactly two good muons. A good muon is defined to be a muon reconstructed in the muon spectrometer with a matched track in the inner detector with transverse momentum above 25 GeV and $|\eta| < 2.5$ [8]. Additional requirements on the number of hits used to reconstruct the tracks in the inner detector are applied. The z displacement of the muon tracks from the primary vertex is required to be less than 10 mm. Isolation criteria are applied around the muon track.

The selection of $Z \to ee$ events requires the presence of exactly two identified electrons with $|\eta| < 2.47$, which pass the "medium" identification criteria [9, 10], optimized for 2012 data, and have transverse momenta above 25 GeV. Electron candidates in the electromagnetic calorimeter transition region, $1.37 < |\eta| < 1.52$, are not considered for this study.

[2]The mean number of inelastic proton proton interactions per bunch is averaged over one luminosity block lasting typically 60 seconds and calculated from the measured instantaneous luminosity, L, the inelastic cross section, σ_{inel}, and the average number of colliding bunch pairs per revolution in the LHC, $N_{bunch} \times f_{LHC}$: $\langle\mu\rangle = L \times \sigma_{inel}/(N_{bunch} \times f_{LHC})$

In both the $Z \to ee$ and the $Z \to \mu\mu$ selections, the two leptons are required to have opposite charge and the reconstructed invariant mass of the di-lepton system, $m_{\ell\ell}$, is required to be consistent with the Z mass, $66 < m_{\ell\ell} < 116\,\text{GeV}$.

3.3 $W \to \ell\nu$ event selection

Lepton candidates are selected with lepton identification criteria similar to those used for the Z selection. An isolation cut is applied around the electron energy deposits in the calorimeter to reduce contamination from jets. The event is required to contain exactly one reconstructed lepton (electron or muon). The $E_{\text{T}}^{\text{miss}}$, calculated as described in Section 5, is required to be greater than 25 GeV. The reconstructed mass of the transverse momentum of the lepton, $\mathbf{p}_{\text{T}}^{\ell}$, and $\boldsymbol{E}_{\text{T}}^{\text{miss}}$, $m_{\text{T}} = \sqrt{2p_{\text{T}}^{\ell}E_{\text{T}}^{\text{miss}}(1-\cos\phi)}$, where ϕ is the azimuthal angle between the lepton momentum and $\boldsymbol{E}_{\text{T}}^{\text{miss}}$ directions, must satisfy $m_{\text{T}} > 50\,\text{GeV}$.

4 Monte Carlo simulation samples

Monte Carlo (MC) samples of $Z \to \ell\ell$ and $W \to \ell\nu$ production are generated with the next-to-leading (NLO) order POWHEG [11] model, with the final state partons showered by the PYTHIA8 program [12, 13], using the CT10 next-to-leading order (NLO) parton distribution function (PDF) [14] and the ATLAS AU2 tune [15]. Samples of $Z \to \ell\ell$ generated with ALPGEN [16] are also used for some additional data-MC comparison. The $t\bar{t}$ events are generated with the MC@NLO program [17]. The $Z \to \tau\tau$ and $H \to \tau\tau$ events with m_H= 125 GeV, from direct production or produced through the Vector Boson Fusion mechanism (VBF $H \to \tau\tau$), are also generated with POWHEG. The performance has also been tested with samples of simulated supersymmetry (SUSY) events. An R-parity conserving simplified model is used, in which pair-production of gluinos is simulated. The gluinos are assumed to decay with unit probability to a top quark, and anti-top quark and a stable invisible neutralino with mass of 1 GeV. Two different values of the gluino mass are used, 0.5 TeV (labelled SUSY500 in what follows) and 1.0 TeV (SUSY1000). These samples were generated using HERWIG++ [18].

Additional inelastic pp interactions, known as pile-up interactions, are generated using the PYTHIA8 program with the ATLAS MC12 A2M tune [15] and the MSTW08 leading order (LO) PDF [19]. The proton-proton bunches are organised in trains, with 50 ns spacing between bunches, closely matching the bunch structure of the LHC. Therefore the simulation contains effects from pile-up arising from bunches before or after the bunch crossing in which the event of interest was triggered (out-of-time pile-up). The MC simulation samples are weighted such that the distribution of the average number of interactions per bunch crossing matches that observed in the 2012 data sample, to ensure that the pile-up interactions are accurately described. When the pile-up conditions are not specified for a given figure, they should be assumed to be matched to those observed in the 2012 data sample used.

The GEANT4 software toolkit [20] within the ATLAS simulation framework [21] simulates the propagation of the generated particles through the ATLAS detector and their interactions with the detector material. It was used for all samples.

The same trigger and event selection criteria used for $Z \to \ell\ell$ and $W \to \ell\nu$ data are also applied to the simulated $Z \to \ell\ell$ and $W \to \ell\nu$ events. The $t\bar{t}$ events are required to contain at least one electron or muon with $p_{\text{T}} > 25\,\text{GeV}$. For $Z \to \tau\tau$ and $H \to \tau\tau$ simulations the lepton-hadron events are selected, where one τ decays to a lepton (electron or muon) and the other to hadrons, requiring an electron or a muon and an identified τ-jet , both with $p_{\text{T}} > 20\,\text{GeV}$.

5 $\boldsymbol{E}_{\mathrm{T}}^{\mathrm{miss}}$ reconstruction and calibration

The $\boldsymbol{E}_{\mathrm{T}}^{\mathrm{miss}}$ reconstruction [1] uses energy deposits in the calorimeters and muons reconstructed in the muon spectrometer. Also muons formed by segments which are matched to inner detector tracks extrapolated to the muon spectrometer (tagged muons) are used to recover muons, typically of low pT, which did not cross enough precision muon chambers to allow an independent momentum measurement in the muon spectrometer. Tracks are added to recover the contribution from low-p_{T} particles which are missed in the calorimeters.

The $\boldsymbol{E}_{\mathrm{T}}^{\mathrm{miss}}$ calculation uses reconstructed and calibrated physics objects. Calorimeter energy deposits are associated with a reconstructed and identified high-p_{T} parent object in a specific order: electrons, photons, hadronically decaying τ-leptons, jets and finally muons. Deposits not associated with any such objects are also taken into account in the $\boldsymbol{E}_{\mathrm{T}}^{\mathrm{miss}}$ calculation. The $\boldsymbol{E}_{\mathrm{T}}^{\mathrm{miss}}$ is calculated as follows:

$$E_{x(y)}^{\mathrm{miss}} = E_{x(y)}^{\mathrm{miss},e} + E_{x(y)}^{\mathrm{miss},\gamma} + E_{x(y)}^{\mathrm{miss},\tau} + E_{x(y)}^{\mathrm{miss,jets}} + E_{x(y)}^{\mathrm{miss,SoftTerm}} + E_{x(y)}^{\mathrm{miss},\mu}, \quad (1)$$

where each term is calculated as the negative sum of the calibrated reconstructed objects, projected onto the x and y directions. Because of the high granularity of the calorimeter, it is important to suppress noise contributions and to use in the $\boldsymbol{E}_{\mathrm{T}}^{\mathrm{miss}}$ calculation, in addition to the high-p_{T} reconstructed objects, only the calorimeter energy deposits containing a significant signal. This is achieved by calculating the $\boldsymbol{E}_{\mathrm{T}}^{\mathrm{miss}}$ soft term using only energy deposits from topological clusters, referred to as topoclusters hereafter [22]. To avoid double counting energy, the parametrized muon energy loss in the calorimeters is subtracted in the $\boldsymbol{E}_{\mathrm{T}}^{\mathrm{miss}}$ calculation if the combined muon momentum is used [1].

In Equation 1, electrons are calibrated with the standard ATLAS electron calibration [10] and photons are calibrated at the electromagnetic scale (EM)[3]. The τ-jets are calibrated with the local cluster weighting (LCW) [23, 24] which involves classifying the energy depositions as electromagnetic or hadronic, and weighting them appropriately when computing the topocluster energy, an offset is subtracted to suppress the pile-up effects, and the tau energy scale (TES) correction [25] is applied. The jets are reconstructed with the anti-k_t algorithm [26], with distance parameter $R = 0.4$. Each jet is corrected for the pile-up and is subsequently calibrated with the LCW+JES scheme, where JES is the jet energy scale [24]. Only jets with calibrated p_{T} greater than 20 GeV are used to calculate the jet term in Equation 1. The soft term[4] is calculated from topoclusters and tracks not associated to high-p_{T} objects (i.e. from unassociated topoclusters and tracks), the topoclusters being calibrated using the LCW technique and removing any overlap between tracks and topoclusters.

The $\boldsymbol{E}_{\mathrm{T}}^{\mathrm{miss}}$ is sometimes described by its azimuthal angle and magnitude, ϕ^{miss} and $E_{\mathrm{T}}^{\mathrm{miss}}$.

The total transverse energy in the calorimeters, $\sum E_{\mathrm{T}}$, which includes also the unassociated low-p_{T} tracks used in the soft term, is an important quantity to parameterise and understand the $\boldsymbol{E}_{\mathrm{T}}^{\mathrm{miss}}$ performance. It is defined as the scalar sum:

$$\sum E_{\mathrm{T}} = \sum E_{\mathrm{T}}^{\mathrm{e}} + \sum E_{\mathrm{T}}^{\gamma} + \sum E_{\mathrm{T}}^{\tau} + \sum E_{\mathrm{T}}^{\mathrm{jets}} + \sum E_{\mathrm{T}}^{\mathrm{SoftTerm}}, \quad (2)$$

which is the scalar sum of the transverse energy of reconstructed and calibrated objects and of the soft term according to the scheme described above for $\boldsymbol{E}_{\mathrm{T}}^{\mathrm{miss}}$. The total transverse energy in the event is

[3] The EM scale is the basic calorimeter signal scale for the ATLAS calorimeters. It provides the correct scale for energy deposited by electromagnetic showers. It does not correct for the lower energy hadron shower response nor for energy losses in the dead material.

[4] It should be noted that the $\boldsymbol{E}_{\mathrm{T}}^{\mathrm{miss,SoftTerm}}$ in Equation 1 includes contributions both from jets with $p_T < 20$ GeV and from unassociated topoclusters/tracks. Previously [1, 2] those contributions were calculated separately, and were denoted as $\boldsymbol{E}_{\mathrm{T}}^{\mathrm{miss,softjets}}$ and $\boldsymbol{E}_{\mathrm{T}}^{\mathrm{miss,CellOut}}$ respectively.

obtained by summing the p_{T} of muons and the $\sum E_{\mathrm{T}}$ in the calorimeters:

$$\sum E_{\mathrm{T}}(\text{event}) = \sum E_{\mathrm{T}} + \sum p_{\mathrm{T}}^{\mu}. \tag{3}$$

6 Methods for pile-up suppression in $\boldsymbol{E}_{\mathrm{T}}^{\mathrm{miss}}$

In Ref. [2], it was shown that a clear deterioration of the performance is observed when the average number of pile-up interactions per event increases. In the same note it was shown that the pile-up affects also the $\boldsymbol{E}_{\mathrm{T}}^{\mathrm{miss}}$ response. Methods to suppress pile-up are therefore needed which can restore the $\boldsymbol{E}_{\mathrm{T}}^{\mathrm{miss}}$ resolution to values more similar to the ones observed in the absence of pile-up, without spoiling the $\boldsymbol{E}_{\mathrm{T}}^{\mathrm{miss}}$ response and without creating fake $\boldsymbol{E}_{\mathrm{T}}^{\mathrm{miss}}$.

All $\boldsymbol{E}_{\mathrm{T}}^{\mathrm{miss}}$ terms in Equations 1 and 2 are affected by pile-up, but the terms which are most affected are the jets and soft term, because the pile-up largely produces hadronic energy and they are reconstructed from larger regions in the calorimeters. Methods for the suppression of pile-up in these terms are summarized in this section.

6.1 Pile-up suppression in the $\boldsymbol{E}_{\mathrm{T}}^{\mathrm{miss}}$ jet term based on tracks

Pile-up not only distorts the energy reconstructed in jets but can also create additional jets. As discussed in Section 5, the jets with $p_{\mathrm{T}}>20\,\mathrm{GeV}$ used in the $\boldsymbol{E}_{\mathrm{T}}^{\mathrm{miss}}$ reconstruction are already corrected for pile-up effects, using the jet area method [27]. The corrected jet p_T^{jetcorr} is calculated as $p_T^{\mathrm{jet}} - \rho \times A^{\mathrm{jet}}$, where ρ is the transverse momentum density in the event, calculated as the median of $p_T^{\mathrm{jet}}/A^{\mathrm{jet}}$ from the jets built with the recursive recombination algorithm k_t [28, 29] with distance parameter $R = 0.4$ in $|\eta| < 2$ and A^{jet} is the area of the jet. This correction captures event-by-event fluctuations and has no dependence on pile-up modeling.

To further suppress the jets originating from pile-up, a cut is applied based on the jet vertex fraction, JVF [30], i.e. the fraction of momenta of tracks matched to the jet which are associated with the hard scattering vertex. JVF is defined as:

$$\mathrm{JVF} = \sum_{\mathrm{tracks_{jet}},\mathrm{PV}} p_{\mathrm{T}} / \sum_{\mathrm{tracks_{jet}}} p_{\mathrm{T}}, \tag{4}$$

where the sums are taken over the tracks matched to the jet and PV denotes the tracks associated to the primary vertex[5]. Only tracks with $p_{\mathrm{T}} > 400\,\mathrm{MeV}$ and passing further quality criteria relating to impact parameters and number of hits in different ID sub-detectors are used to make primary vertices. Jets with no associated tracks are assigned JVF = −1. Within this note, any jet with $p_{\mathrm{T}} < 50\,\mathrm{GeV}$ and with $|\eta| < 2.4$ which does not satisfy $|\mathrm{JVF}| > 0$ is discarded in the calculation of the pile-up suppressed $E_{\mathrm{T}}^{\mathrm{miss,jets}}$. This requirement, which discards only those jets, inside the tracker acceptance $|\eta| < 2.4$, which have no tracks originating from the leading primary vertex, reduces the jets originating from pile-up. Jets with no associated tracks, which have JVF = −1 and include all jets outside the inner detector region, are kept.

6.2 Pile-up suppression in the $\boldsymbol{E}_{\mathrm{T}}^{\mathrm{miss}}$ soft term based on tracks

The pile-up largely affects the soft term. Since the $\boldsymbol{E}_{\mathrm{T}}^{\mathrm{miss,SoftTerm}}$ can have an important contribution to the momentum balance in the event, completely neglecting its contribution in the $\boldsymbol{E}_{\mathrm{T}}^{\mathrm{miss}}$ reconstruction

[5] Defined as the primary vertex that has maximal $\sum {p_{\mathrm{T}}}^2$ of the tracks associated with it.

gives a poorer performance [2]. Two different methods for suppressing the pile-up in the soft term are described in the following, one based on the use of tracks and the other one based on the jet area method.

Tracks provide an excellent method for pile-up suppression, since they can be associated with the primary vertex from the hard scattering collision. Pile-up suppression is achieved by scaling the $\boldsymbol{E}_{\mathrm{T}}^{\mathrm{miss,SoftTerm}}$ with the soft term vertex fraction (STVF) i.e. the fraction of momenta of tracks matched to the soft term which are associated with the hard scattering vertex. It is calculated, in a similar way as JVF, as:

$$\mathrm{STVF} = \sum_{\mathrm{tracks}_{\mathrm{SoftTerm}},\mathrm{PV}} p_{\mathrm{T}} / \sum_{\mathrm{tracks}_{\mathrm{SoftTerm}}} p_{\mathrm{T}}, \tag{5}$$

where the sums are taken over the tracks unmatched to physics objects and PV denotes the tracks associated to the primary vertex.

The $\boldsymbol{E}_{\mathrm{T}}^{\mathrm{miss,SoftTerm}}$ is multiplied by the STVF factor and the $\boldsymbol{E}_{\mathrm{T}}^{\mathrm{miss}}$ calculated with this corrected soft term is named STVF.

6.3 Pile-up suppression in the $\boldsymbol{E}_{\mathrm{T}}^{\mathrm{miss}}$ soft term using the jet area method

This method for the pile-up subtraction in the $\boldsymbol{E}_{\mathrm{T}}^{\mathrm{miss,SoftTerm}}$ is based on the jet area, which is also the correction used for jets described in Section 6.1. The essential ingredients are:

- the reclustering of the energy from topoclusters and tracks entering in the $\boldsymbol{E}_{\mathrm{T}}^{\mathrm{miss,SoftTerm}}$. For this task, jets are reconstructed down to $p_{\mathrm{T}} = 0$ using the k_t algorithm
- the event transverse momentum density ρ is used to determine the contribution due to pile-up in the jet area, which is subtracted from each k_t jet: $p_T^{\mathrm{jetcorr}} = p_T^{\mathrm{jet}} - \rho \times A^{\mathrm{jet}}$. The $p_T^{\mathrm{jetcorr}} = 0$ if $p_T^{\mathrm{jet}} < \rho \times A^{\mathrm{jet}}$
- finally a track-based filter is applied to k_t jets, similar to the one used for jets, and the $\boldsymbol{E}_{\mathrm{T}}^{\mathrm{miss,SoftTerm}}$ is calculated using only the k_t jets after pile-up subtraction which satisfy $|\mathrm{JVF}| > 0.25$.

Two different $\boldsymbol{E}_{\mathrm{T}}^{\mathrm{miss,SoftTerm}}$ calculations are considered in this note and the $\boldsymbol{E}_{\mathrm{T}}^{\mathrm{miss}}$ is then recalculated using each of them. The two methods differ only in their calculation of the ρ, as follows:

- the ρ is calculated as the median of $p_T^{\mathrm{jet}}/A^{\mathrm{jet}}$ from the k_t jets ($R = 0.4$) reconstructed from topoclusters and tracks associated to the soft term in $|\eta| < 1.8$ (plateau region) and extrapolated to the forward region using the ρ shape as a function of η, determined from minimum bias events in the 2012 data. The distribution of $\rho(\eta)$ is fitted with an analytic function, obtained by summing two gaussians, one for the plateau region (depending on the $\sum E_{\mathrm{T}}$ of the event) and the other for the forward region (whose parameters depend on $\langle\mu\rangle$ of the events). The soft term jets are formed using the k_t algorithm with $R = 0.6$ and they are corrected and filtered as explained above. The corresponding $\boldsymbol{E}_{\mathrm{T}}^{\mathrm{miss}}$ is named Extrapolated Jet Area Filtered.
- the ρ is calculated as the median of $p_T^{\mathrm{jet}}/A^{\mathrm{jet}}$ from the k_t jets ($R = 0.8$) reconstructed from topoclusters and tracks associated to the soft term in $|\eta| < 5$. The soft term jets are formed using the k_t algorithm with $R = 0.4$ and they are corrected and filtered as explained above. The corresponding $\boldsymbol{E}_{\mathrm{T}}^{\mathrm{miss}}$ is named Jet Area Filtered.

6.4 Definitions

In the following sections, the performances of the $\boldsymbol{E}_{\mathrm{T}}^{\mathrm{miss}}$ reconstruction before and after the pile-up suppression are shown for the different methods based on tracks or using jet area, in terms of resolution,

response and tails for data and MC events. Four $\boldsymbol{E}_{\mathrm{T}}^{\mathrm{miss}}$ calculations are compared, one without a special pile-up suppression treatment and three with pile-up mitigation techniques applied. They differ only in the soft term and the jet term.

- the $\boldsymbol{E}_{\mathrm{T}}^{\mathrm{miss}}$ **before pile-up suppression** has the jet term calculated from all jets with $p_{\mathrm{T}}> 20\,\mathrm{GeV}$ corrected with jet area and the soft term calculated from unassociated topoclusters and tracks, as described in Section 5.

- the three pile-up suppressed variants have the same jet term formed from all jets (corrected with jet area) with $p_{\mathrm{T}}> 50\,\mathrm{GeV}$ and from the ones with $20 < p_{\mathrm{T}} < 50\,\mathrm{GeV}$ and $|\eta|< 2.4$ with $|\mathrm{JVF}| > 0$. They differ in the soft term as described in this section; one uses the track based STVF weight ($\boldsymbol{E}_{\mathrm{T}}^{\mathrm{miss}}$ **STVF**) and the two others use the jet area pile-up suppression ($\boldsymbol{E}_{\mathrm{T}}^{\mathrm{miss}}$ **Extrapolated Jet Area Filtered** and **Jet Area Filtered**).

7 Study of $\boldsymbol{E}_{\mathrm{T}}^{\mathrm{miss}}$ performance in different event topologies

7.1 Characterization of samples used for the study of $\boldsymbol{E}_{\mathrm{T}}^{\mathrm{miss}}$ performance

The $\boldsymbol{E}_{\mathrm{T}}^{\mathrm{miss}}$ performance depends on the event topology, i.e. presence of genuine $\boldsymbol{E}_{\mathrm{T}}^{\mathrm{miss}}$, presence of leptons, jet activity, etc. The values of quantities relevant for $\boldsymbol{E}_{\mathrm{T}}^{\mathrm{miss}}$ studies in the MC samples used in this note are shown in Figure 1 and Figure 2. In Figure 1 the reconstructed $E_{\mathrm{T}}^{\mathrm{miss}}$ and $\sum E_{\mathrm{T}}$ before and after pile-up suppression are compared with the true values. As can be seen, the $\sum E_{\mathrm{T}}$ is strongly suppressed by all the pile-up suppression methods and it is closer to the true value. The average number of jets before and after the pile-up suppression (JVF cut) is also shown. Figure 2 shows the importance of the soft term and of the jet term in the different samples. The average value of $E_{\mathrm{T}}^{\mathrm{miss,SoftTerm}}$ is not much different in the various samples but its contribution is dominant in Z samples and important in W events, while it becomes less important in events with higher jet multiplicity, where the $E_{\mathrm{T}}^{\mathrm{miss,jets}}$ is dominant, as can be seen from the distribution of the ratios of $\sum E_{\mathrm{T}}^{\mathrm{SoftTerm}}/\sum E_{\mathrm{T}}$ and $\sum E_{\mathrm{T}}^{\mathrm{jets}}/\sum E_{\mathrm{T}}$.

7.2 Comparison of $\boldsymbol{E}_{\mathrm{T}}^{\mathrm{miss}}$ distributions in data and MC simulation

In this section some basic distributions in $Z \to \ell\ell$ and $W \to \ell\nu$ events from data are compared with the expected distributions from the MC samples, before and after pile-up suppression. The comparison is done also separately for each of the various terms in Equations 1 and 2.

7.2.1 $\boldsymbol{E}_{\mathrm{T}}^{\mathrm{miss}}$ distributions in $\boldsymbol{Z \to \ell\ell}$ events

The $Z \to \ell\ell$ channel is well-suited to the study of $\boldsymbol{E}_{\mathrm{T}}^{\mathrm{miss}}$ performance because of its clean event signature and the relatively large cross-section. In general, apart from a small contribution from the semi-leptonic decay of heavy-flavour hadrons in jets or background contributions, no genuine $E_{\mathrm{T}}^{\mathrm{miss}}$ is expected in these events. Thus most of the $\boldsymbol{E}_{\mathrm{T}}^{\mathrm{miss}}$ reconstructed in these events is a direct result of imperfections in the reconstruction process or in the detector response.

The distributions of $E_{\mathrm{T}}^{\mathrm{miss}}$ for data are shown in Figure 3 for $Z \to \mu\mu$ events. The MC simulation expectations, from $Z \to \mu\mu$ events and from the dominant backgrounds, are superimposed. Each MC sample is weighted with its corresponding cross-section and then the total MC expectation is normalized to the number of events in data. A good agreement between data and MC simulation is observed in the $E_{\mathrm{T}}^{\mathrm{miss}}$ distribution, both before and after pile-up suppression. The tails in the $E_{\mathrm{T}}^{\mathrm{miss}}$ distribution in $Z \to \ell\ell$ data are compatible with either signal candidates or with backgrounds, including $t\bar{t}$ and di-boson events, all involving real $E_{\mathrm{T}}^{\mathrm{miss}}$, demonstrating that the instrumental effects are well described.

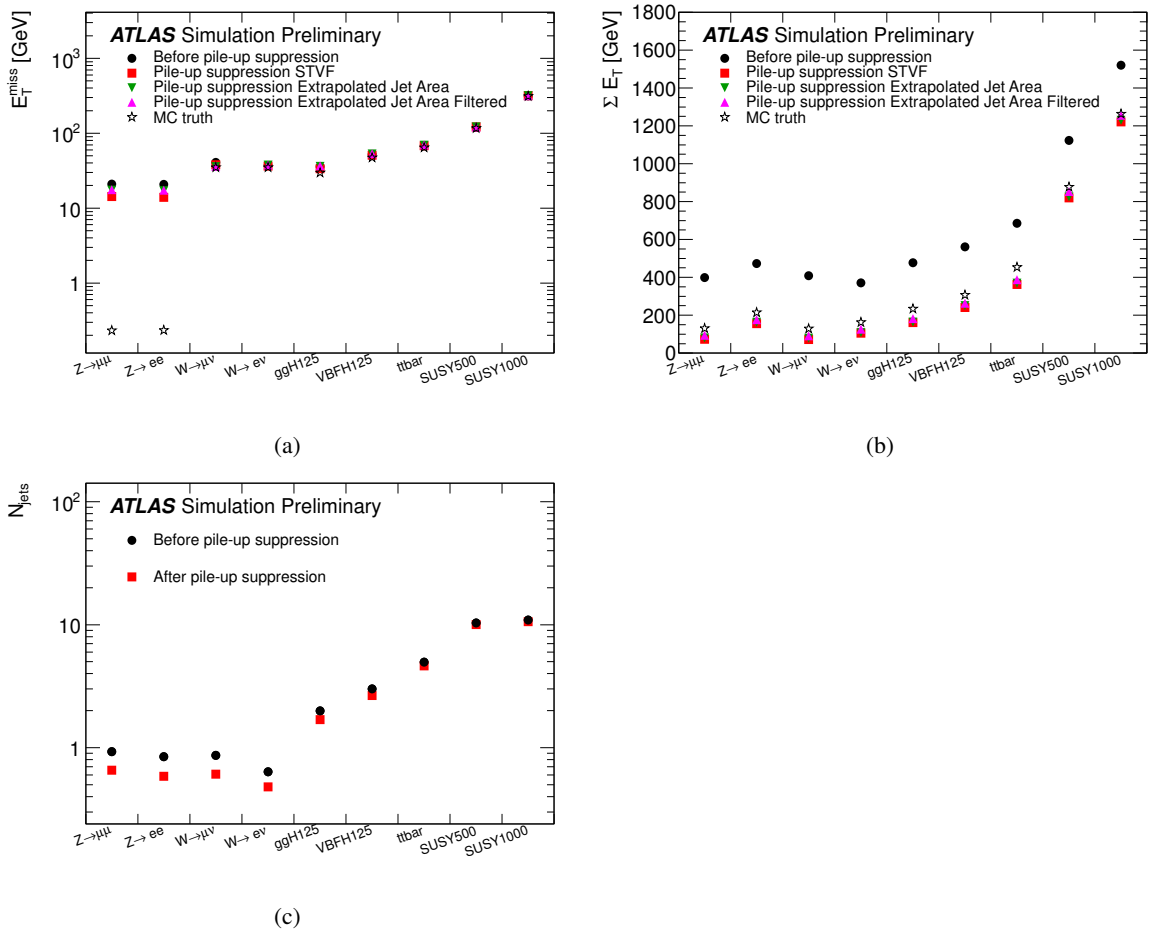

(a)

(b)

(c)

Figure 1: *Average values of E_T^{miss} (a), $\sum E_T$ (b) and of the number of jets with $p_T >$ 20 GeV (c) in the MC samples used. The values before pile-up suppression and the values after pile-up suppression with different methods are shown. The true MC values are also shown in (a) and (b).*

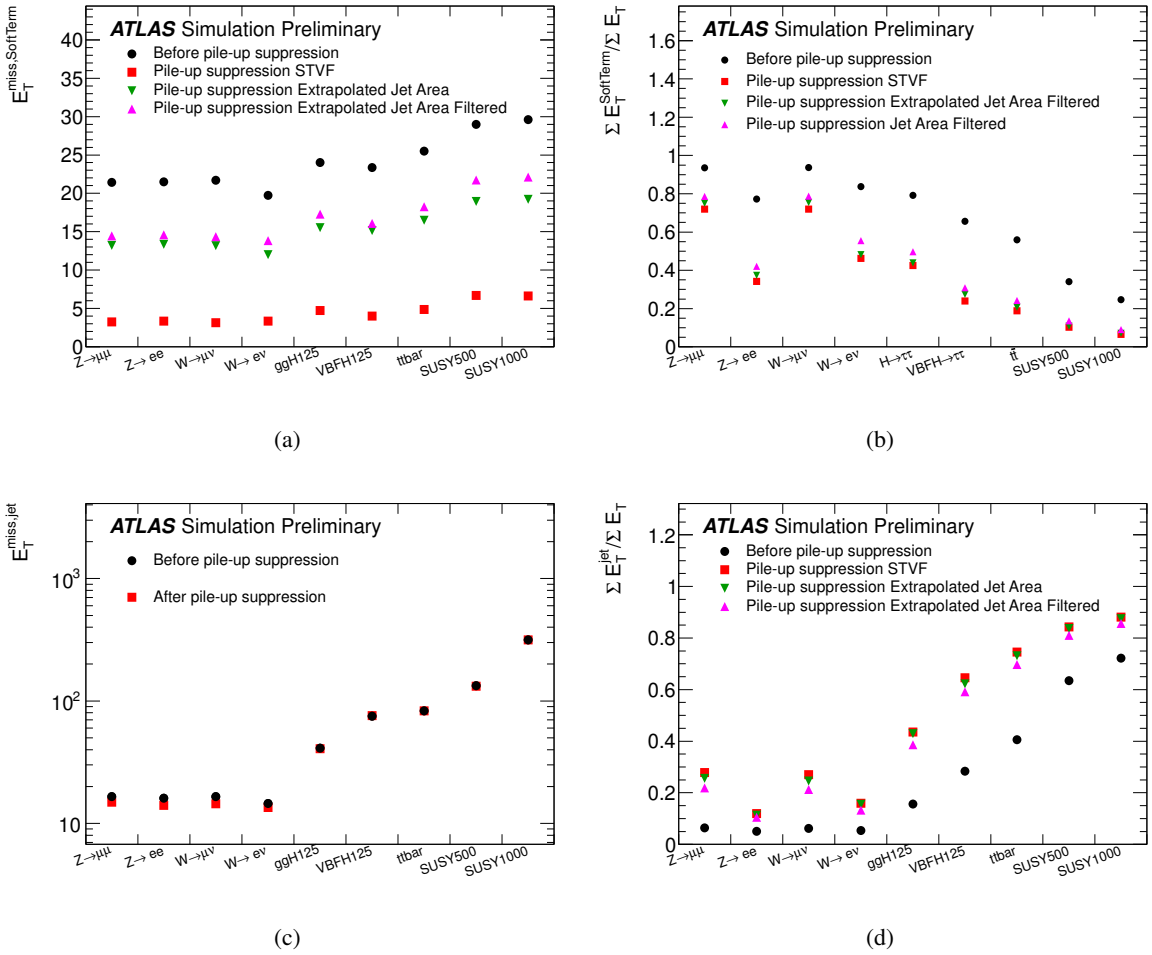

Figure 2: $E_T^{miss,SoftTerm}$ *(a), ratio of* $\sum E_T^{SoftTerm}$ *over* $\sum E_T$ *(b),* $E_T^{miss,jets}$ *(c) and ratio of* $\sum E_T^{jets}$ *over* $\sum E_T$ *(d) in the samples used. The values before pile-up suppression and after pile-up suppression are shown.*

The contributions to $\boldsymbol{E}_{\mathrm{T}}^{\mathrm{miss}}$ from jets before and after applying the JVF cut and from reconstructed muons are shown separately in Figure 4. The peak at zero in the distribution of the jet term corresponds to events where there are no jets with p_{T} above 20 GeV, and the small values (< 20 GeV) in the distribution are due to events with two or more jets whose transverse momenta partially balance. The agreement for the jet term is within 20% both before and after pile-up suppression. After pile-up suppression, some more disagreement is observed in the region below 20 GeV populated by events with two or more jets. This is probably due to the poor modeling of the number of additional jets in the MC simulation. The contributions to $\boldsymbol{E}_{\mathrm{T}}^{\mathrm{miss}}$ from the $E_{\mathrm{T}}^{\mathrm{miss,SoftTerm}}$ before and after pile-up suppression are shown in Figure 5. The data-MC agreement for the $E_{\mathrm{T}}^{\mathrm{miss,SoftTerm}}$ is slightly worse after pile-up suppression, due to some discrepancy observed in the STVF fraction, which suffers from the mis-modeling of the track activity in MC simulation.

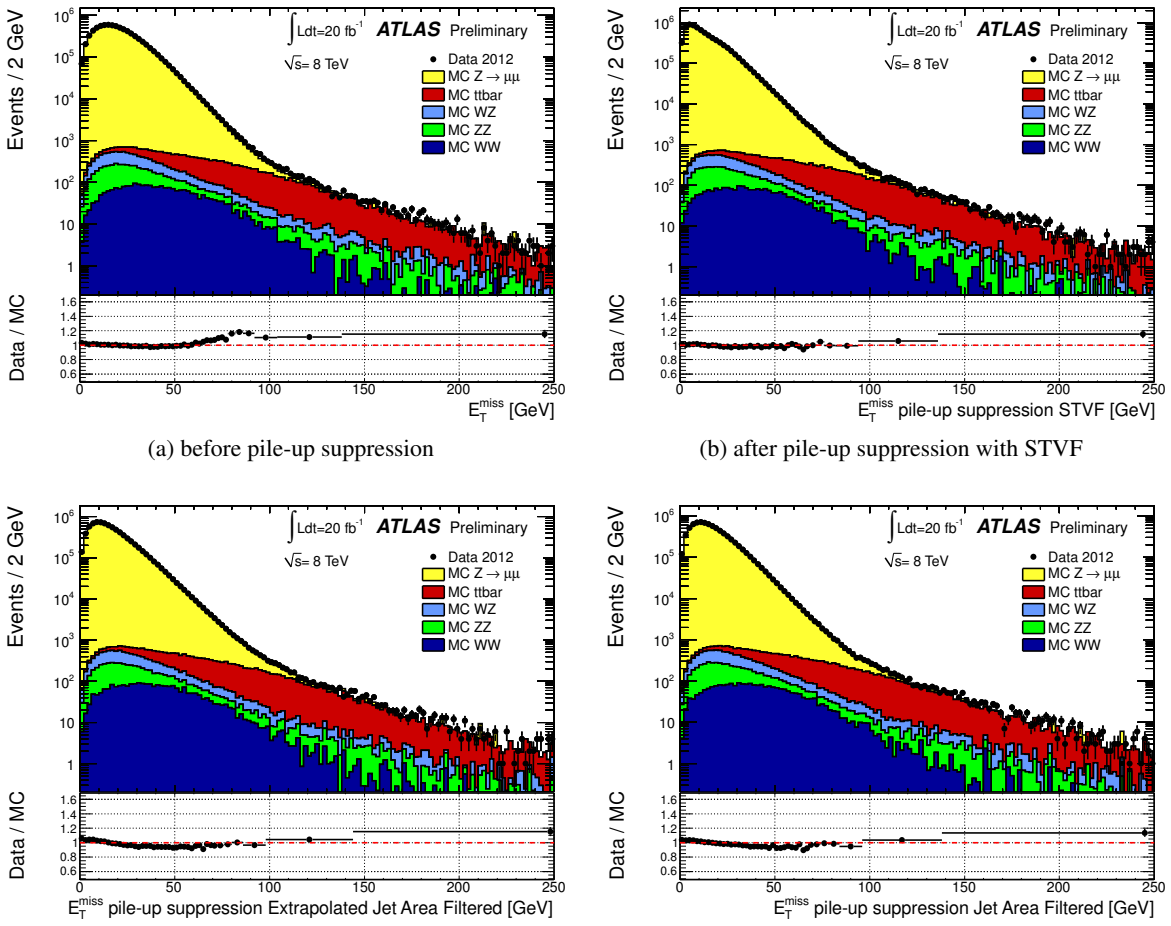

(a) before pile-up suppression

(b) after pile-up suppression with STVF

(c) pile-up suppression Extrapolated Jet Area Filtered

(d) pile-up suppression Jet Area Filtered

Figure 3: *Distribution of E_T^{miss} (a) as measured in a data sample of $Z \rightarrow \mu\mu$ events before pile-up suppression. Distributions of E_T^{miss} after pile-up suppression with the STVF (b), with the Extrapolated Jet Area Filtered (c) and with the Jet Area Filtered (d) methods. The expectation from Monte Carlo simulation is superimposed and normalized to data, after each MC sample is weighted with its corresponding cross-section. The lower parts of the figures show the ratio of data over MC.*

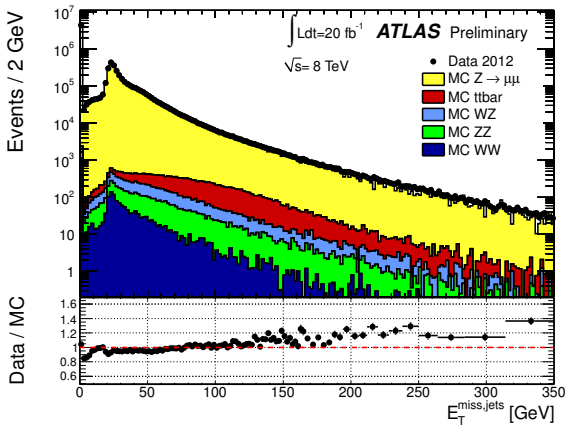

(a) before pile-up suppression

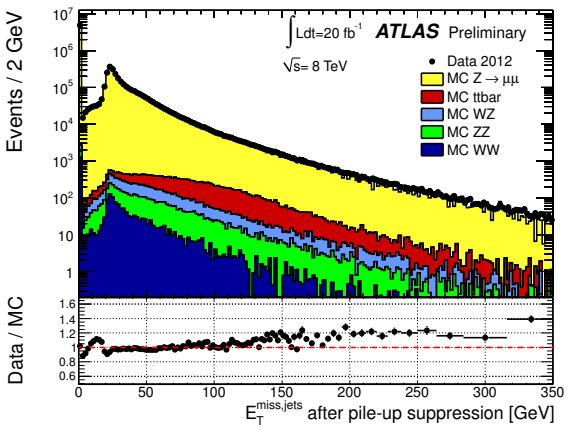

(b) after pile-up suppression with JVF

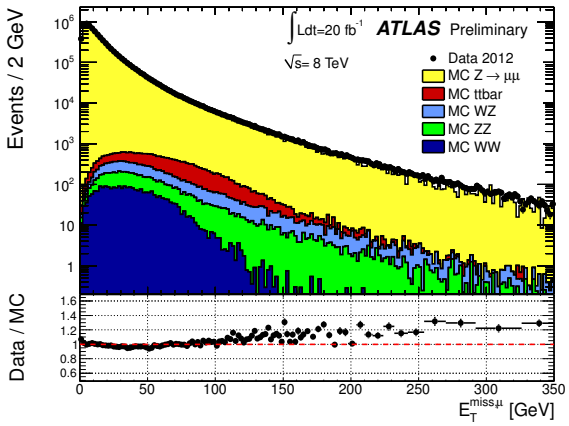

(c) before pile-up suppression

Figure 4: *Distribution of E_T^{miss} computed from reconstructed jets with $p_T > 20\,GeV$ ($E_T^{miss,jets}$) (a), after pile-up suppression with JVF (b) for $Z \rightarrow \mu\mu$ data. The contribution from the muons ($E_T^{miss,\mu}$) is shown separately in (c). The expectation from Monte Carlo simulation is superimposed and normalized to data, after each MC sample is weighted with its corresponding cross-section. The lower parts of the figures show the ratio of data over MC.*

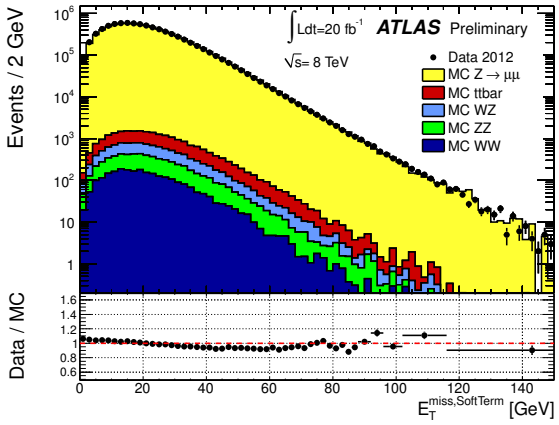

(a) before pile-up suppression

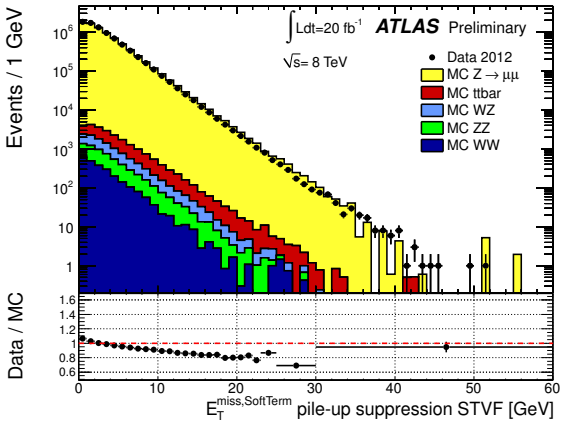

(b) after pile-up suppression with STVF

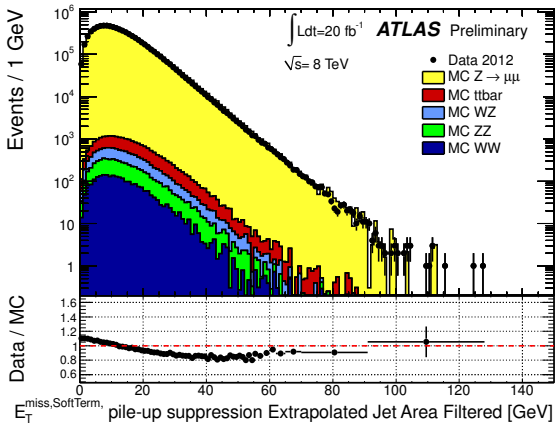

(c) pile-up suppression Extrapolated Jet Area Filtered

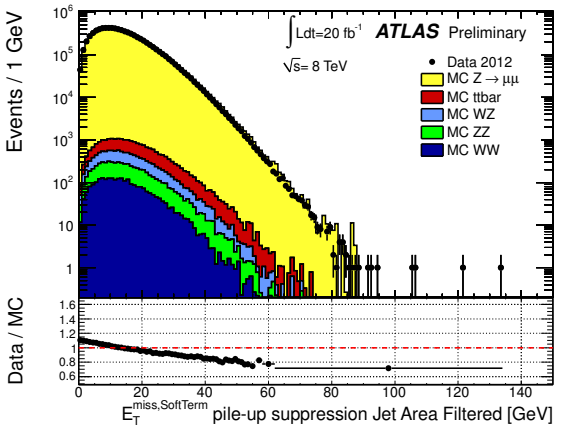

(d) pile-up suppression Jet Area Filtered

Figure 5: *Distribution of $E_T^{miss,SoftTerm}$ before pile-up suppression (a), corrected with STVF (b), corrected with Extrapolated Jet Area Filtered (c) and corrected with Jet Area Filtered (d) for $Z \rightarrow \mu\mu$ data. The expectation from Monte Carlo simulation is superimposed and normalized to data, after each MC sample is weighted with its corresponding cross-section. The lower parts of the figures show the ratio of data over MC.*

7.2.2 $\sum E_{\mathrm{T}}$ distributions in $Z \to \ell\ell$ events

The distributions of $\sum E_{\mathrm{T}}$ for data are shown in Figure 6 for $Z \to \mu\mu$ events. Some data-MC disagreement is observed in the $\sum E_{\mathrm{T}}$ distribution at values below $\sim 200\,\mathrm{GeV}$ and especially above $\sim 600\,\mathrm{GeV}$ before pile-up suppression, while the disagreement is larger after pile-up suppression, which has a large effect on the $\sum E_{\mathrm{T}}$. The distributions of $\sum E_{\mathrm{T}}^{\mathrm{jets}}$ and of $\sum E_{\mathrm{T}}^{\mathrm{SoftTerm}}$ are shown in Figure 7 and 8, respectively. The discrepancy in the $\sum E_{\mathrm{T}}$ distribution is mainly due to the discrepancy in the $\sum E_{\mathrm{T}}^{\mathrm{jets}}$ because of the mis-modeling of the number of jets in the POWHEG+PYTHIA8 MC simulation of the hard process, while there is a better agreement in the $\sum E_{\mathrm{T}}^{\mathrm{SoftTerm}}$ distribution. The discrepancy observed in the $\sum E_{\mathrm{T}}$ distribution becomes more evident after pile-up suppression because of the strong pile-up suppression applied to the soft term.

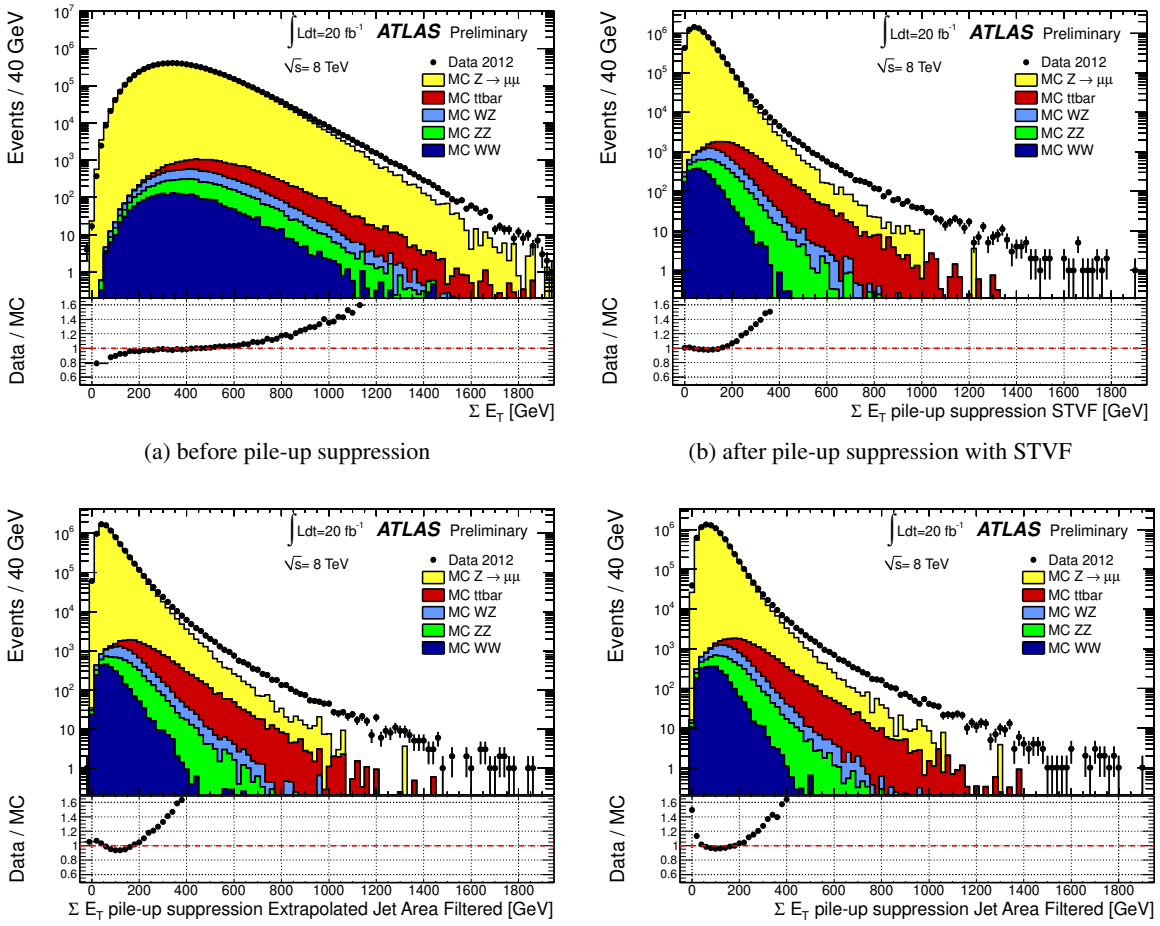

(a) before pile-up suppression

(b) after pile-up suppression with STVF

(c) pile-up suppression Extrapolated Jet Area Filtered

(d) pile-up suppression Jet Area Filtered

Figure 6: *Distribution of $\sum E_T$ as measured in a data sample of $Z \to \mu\mu$ events before pile-up suppression (a), after pile-up suppression with the STVF (b), with the Extrapolated Jet Area Filtered (c) and with the Jet Area Filtered (d) methods. The expectation from Monte Carlo simulation is superimposed and normalized to data, after each MC sample is weighted with its corresponding cross-section. The lower parts of the figures show the ratio of data over MC.*

It is interesting to notice that using the ALPGEN MC event generator the data-MC agreement for the $\sum E_{\mathrm{T}}$ distribution improves, as shown in Figure 9, which is to be compared with Figure 6. This can be

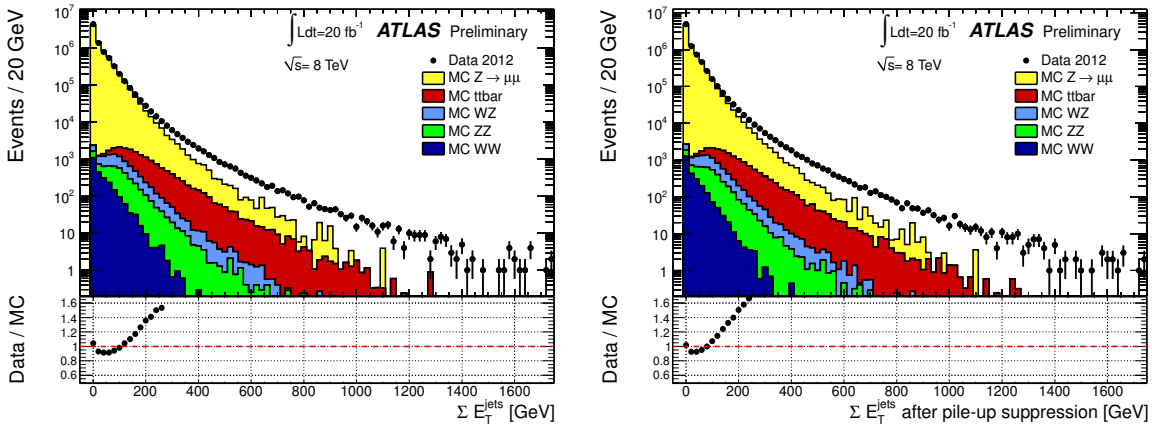

(a) before pile-up suppression

(b) after pile-up suppression with JVF

Figure 7: *Distribution of $\sum E_T$ computed from jets with $p_T > 20\,GeV$ ($\sum E_T^{jets}$) before pile-up suppression (a) and after pile-up suppression with JVF (b) for $Z \to \mu\mu$ data. The expectation from Monte Carlo simulation is superimposed and normalized to data, after each MC sample is weighted with its corresponding cross-section. The lower parts of the figures show the ratio of data over MC.*

explained by a more precise description of jet multiplicity with respect to POWHEG+PYTHIA8 which results in a better data-MC agreement for the $\sum E_{\mathrm{T}}^{\mathrm{jets}}$ as shown in Figure 10, which is to be compared with Figure 7. Figure 11, which is to be compared with Figure 8, shows the distributions of $\sum E_{\mathrm{T}}^{\mathrm{SoftTerm}}$ using the ALPGEN MC. While before pile-up suppression there is a similar data-MC agreement as in Figure 8, which is expected because the soft term is dominated by the pile-up and the pile-up simulation is the same, after pile-up suppression there is a larger data-MC disagreement for ALPGEN, but this does not affect much the global $\sum E_{\mathrm{T}}$ distribution, due to the strong suppression of $\sum E_{\mathrm{T}}^{\mathrm{SoftTerm}}$ after pile-up.

Finally, the distributions of the ratio $E_{\mathrm{T}}^{\mathrm{miss}}/\sqrt{\Sigma E_{\mathrm{T}}}$, are shown in Figure 12. This ratio is an interesting quantity because it has been used as an estimator of the $\boldsymbol{E}_{\mathrm{T}}^{\mathrm{miss}}$ significance in the absence of pile-up. There is a data-MC agreement at the 20% level in the distributions of this ratio both before and after pile-up suppression.

7.2.3 $W \to \ell\nu$ events

In this section the $\boldsymbol{E}_{\mathrm{T}}^{\mathrm{miss}}$ performance is studied in $W \to \ell\nu$ events. In these events genuine $E_{\mathrm{T}}^{\mathrm{miss}}$ is expected due to the presence of the neutrino, therefore the $E_{\mathrm{T}}^{\mathrm{miss}}$ scale can be checked.

The distributions of $E_{\mathrm{T}}^{\mathrm{miss}}$ and $\sum E_{\mathrm{T}}$ in data and in MC simulation are shown in Figure 13 for $W \to e\nu$ events. There is a data-MC discrepancy in the $E_{\mathrm{T}}^{\mathrm{miss}}$ distribution larger than that found in $Z \to \mu\mu$ (shown in Figure 3), which may in part be due to the fact that the QCD background, which should predominantly populate the region of low $E_{\mathrm{T}}^{\mathrm{miss}}$, is not included in the MC expectations shown. A discrepancy is also observed in the $\sum E_{\mathrm{T}}$ distribution.

7.3 $\boldsymbol{E}_{\mathrm{T}}^{\mathrm{miss}}$ resolution

A first study of the $\boldsymbol{E}_{\mathrm{T}}^{\mathrm{miss}}$ resolution is performed using the ratio:

$$R = \mathrm{RMS}(E_{\mathrm{T}}^{\mathrm{miss}}/E_{\mathrm{T}}^{\mathrm{miss,True}})/\langle E_{\mathrm{T}}^{\mathrm{miss}}/E_{\mathrm{T}}^{\mathrm{miss,True}}\rangle \quad (6)$$

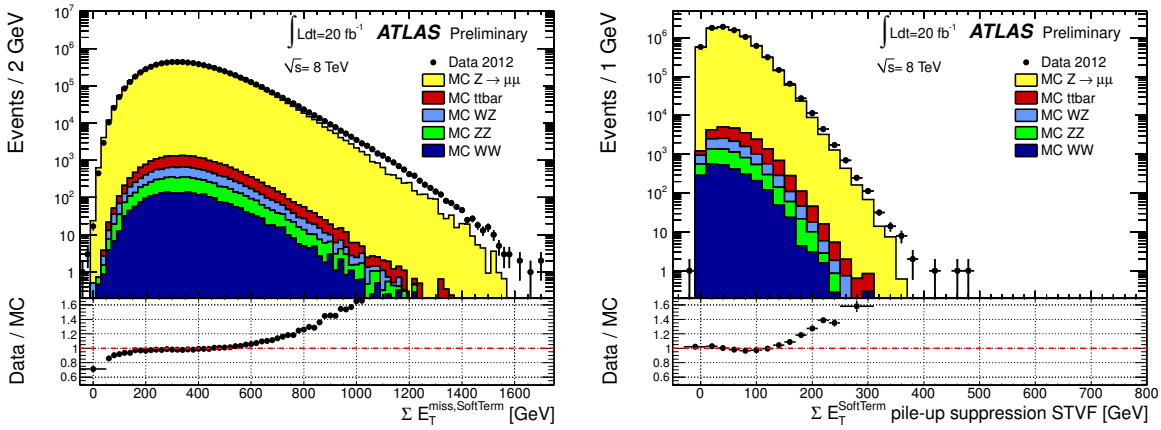

(a) before pile-up suppression

(b) after pile-up suppression with STVF

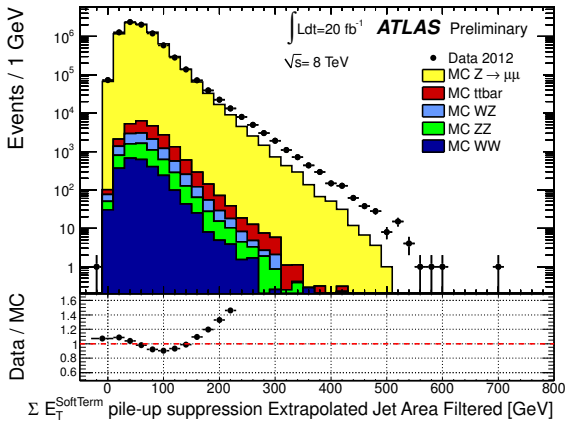

(c) pile-up suppression Extrapolated Jet Area Filtered

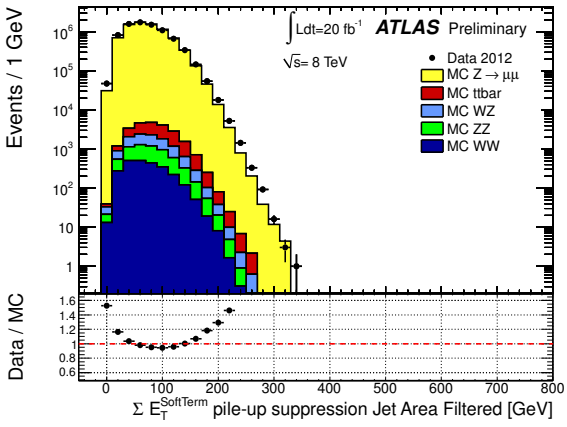

(d) pile-up suppression Jet Area Filtered

Figure 8: *Distribution of* $\sum E_T^{SoftTerm}$ *before pile-up suppression (a), corrected with STVF (b), corrected with Extrapolated Jet Area Filtered (c) and corrected with Jet Area Filtered (d) for* $Z \rightarrow \mu\mu$ *data. The expectation from Monte Carlo simulation is superimposed and normalized to data, after each MC sample is weighted with its corresponding cross-section. The lower parts of the figures show the ratio of data over MC.*

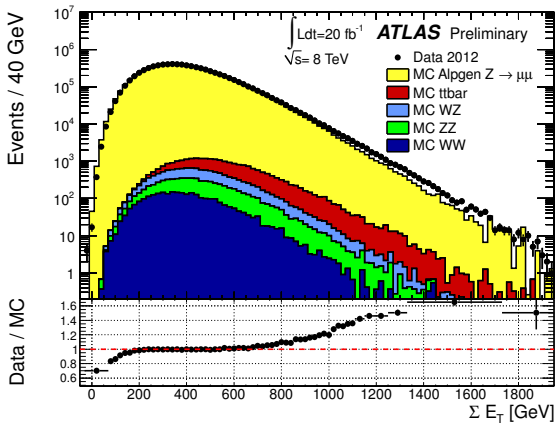

(a) before pile-up suppression

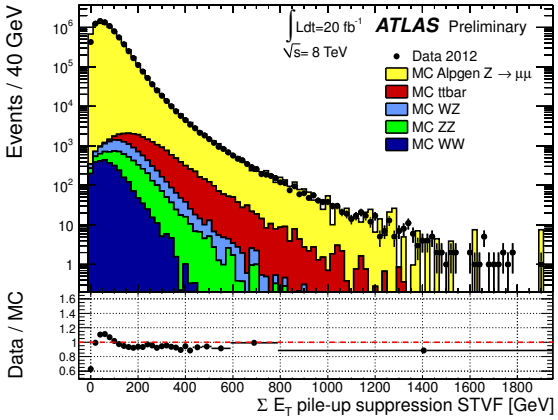

(b) after pile-up suppression with STVF

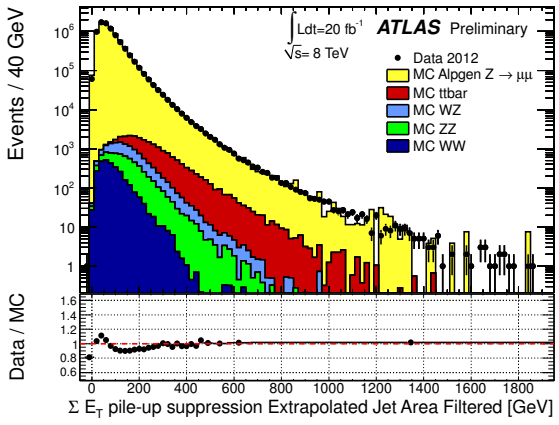

(c) pile-up suppression Extrapolated Jet Area Filtered

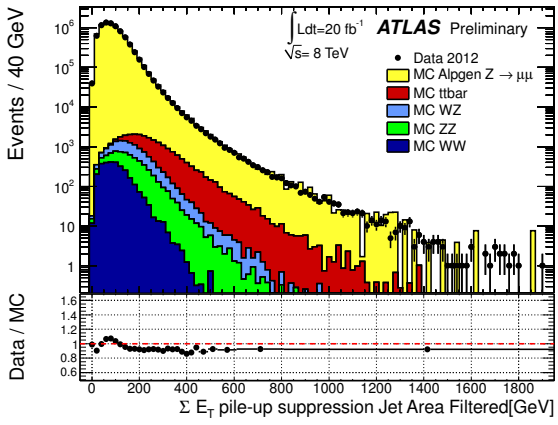

(d) pile-up suppression Jet Area Filtered

Figure 9: *Distribution of $\sum E_T$, as measured in a data sample of $Z \to \mu\mu$ events before pile-up suppression (a), after pile-up suppression with the STVF (b), with the Extrapolated Jet Area Filtered (c) and with the Jet Area Filtered (d) methods. The expectation from Monte Carlo simulation (*ALPGEN*) is superimposed and normalized to data, after each MC sample is weighted with its corresponding cross-section. The lower parts of the figures show the ratio of data over MC.*

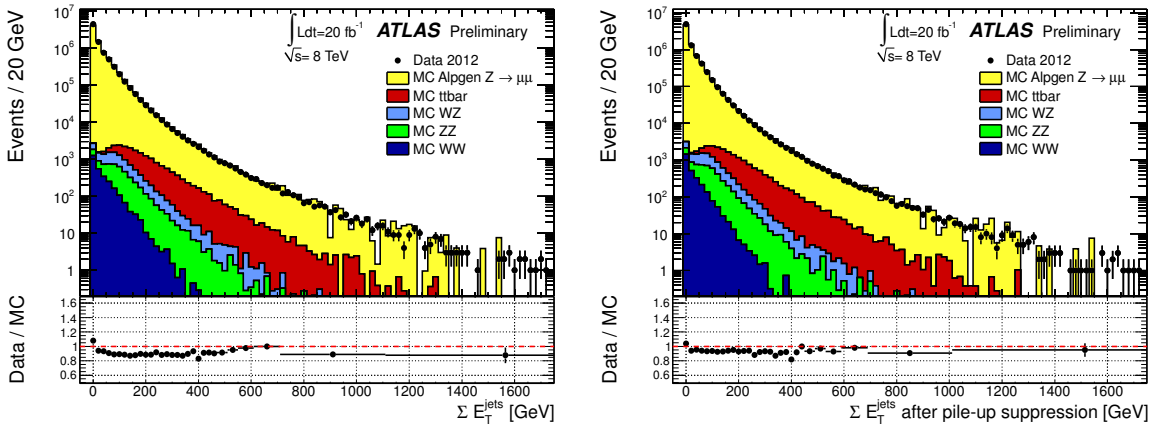

(a) before pile-up suppression

(b) after pile-up suppression with JVF

Figure 10: *Distribution of* $\sum E_T$*, computed from jets with* $p_T > 20\,GeV$ ($\sum E_T^{jets}$) *(a) and after pile-up suppression with JVF (b) for* $Z \to \mu\mu$ *data before pile-up suppression. The expectation from Monte Carlo simulation (*ALPGEN*) is superimposed and normalized to data, after each MC sample is weighted with its corresponding cross-section. The lower parts of the figures show the ratio of data over MC.*

Figure 14 shows the ratio R for different samples. Before pile-up suppression, R decreases with increasing $E_T^{\text{miss,True}}$ and is of the order of 0.1 for larger $E_T^{\text{miss,True}}$ values in all samples. After pile-up suppression, in $W \to \ell\nu$ events, there is a reduction of R in the region of $E_T^{\text{miss,True}} < 40\,\text{GeV}$, while the improvement of R is smaller for larger $E_T^{\text{miss,True}}$ values. In the low $E_T^{\text{miss,True}}$ region there are some concurrent effects: the region is mostly populated by events without jets, so the reduction of R indicates that the pile-up suppression methods in the soft term improve the $\boldsymbol{E}_{\text{T}}^{\text{miss}}$ resolution. Furthermore, in this region, up to about 30-40 GeV, the reconstructed $E_{\text{T}}^{\text{miss}}$ is typically larger than the $E_T^{\text{miss,True}}$, due to the $\boldsymbol{E}_{\text{T}}^{\text{miss}}$ finite resolution, while it becomes smaller than the $E_T^{\text{miss,True}}$ when the $E_T^{\text{miss,True}}$ increases, because of the strong pile-up suppression in the soft term.

This reduction of R after pile-up suppression is not visible in VBF $H \to \tau\tau$ events and in $t\bar{t}$ events, due to the enhanced jet production. There is a very small difference before and after pile-up suppression in the region above 50 GeV which is dominated by high-p_{T} jets to which the JVF cut is not applied.

The resolution of the two $\boldsymbol{E}_{\text{T}}^{\text{miss}}$ components is studied from the width of (E_x^{miss} -$E_x^{\text{miss,True}}$, E_y^{miss} -$E_y^{\text{miss,True}}$). In $Z \to \ell\ell$ events, as well as in minimum bias and jet events, no genuine $E_{\text{T}}^{\text{miss}}$ is expected, so the resolution of the two $\boldsymbol{E}_{\text{T}}^{\text{miss}}$ components is measured in data directly from reconstructed quantities, assuming that the true values of E_x^{miss} and E_y^{miss} are equal to zero.

The distributions of E_x^{miss} -$E_x^{\text{miss,True}}$ in MC $Z \to \mu\mu$ and $W \to e\nu$ events are shown in Figure 15. The distributions of E_y^{miss} -$E_y^{\text{miss,True}}$, not shown, look similar. As can be seen, the pile-up suppression methods improve the resolution of the core of the distributions.

7.3.1 $\boldsymbol{E}_{\text{T}}^{\text{miss}}$ resolution as a function of $\sum E_{\text{T}}$ in different channels

A very good test of the pile-up suppression methods is the study of the stability of the resolution as a function of the number of primary vertices (having more than 2 associated tracks), N_{pv}, which gives an estimation of the in-time pile-up, and $\langle\mu\rangle$, which gives an estimation of the out-of-time pile-up. In this section the resolution of the two $\boldsymbol{E}_{\text{T}}^{\text{miss}}$ components is studied as a function of $\sum E_{\text{T}}$.

The resolution is estimated from the width of the combined distribution of the resolutions of the two

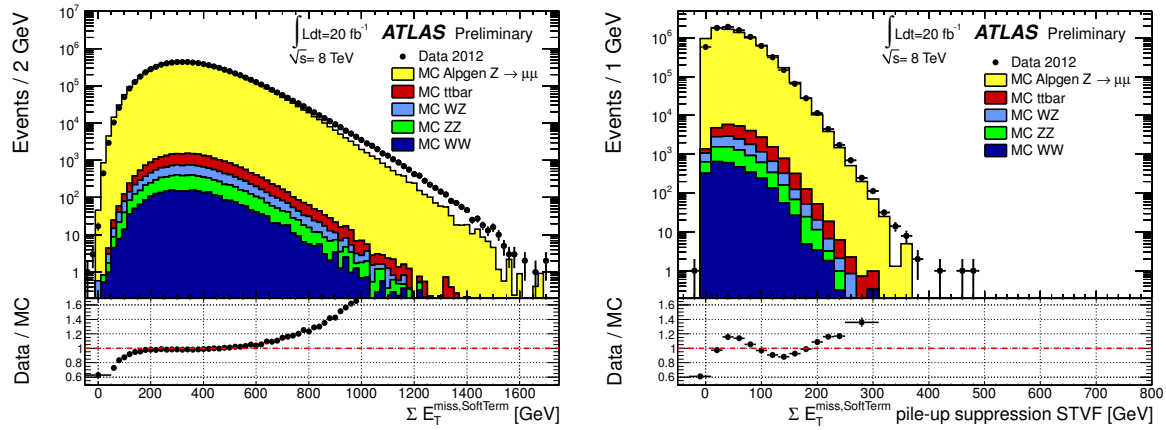

(a) before pile-up suppression

(b) after pile-up suppression with STVF

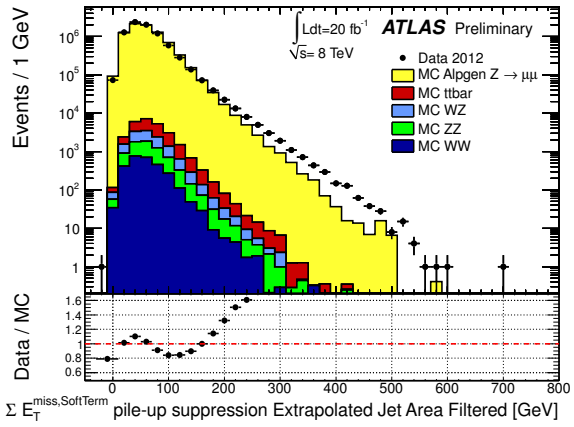

(c) pile-up suppression Extrapolated Jet Area Filtered

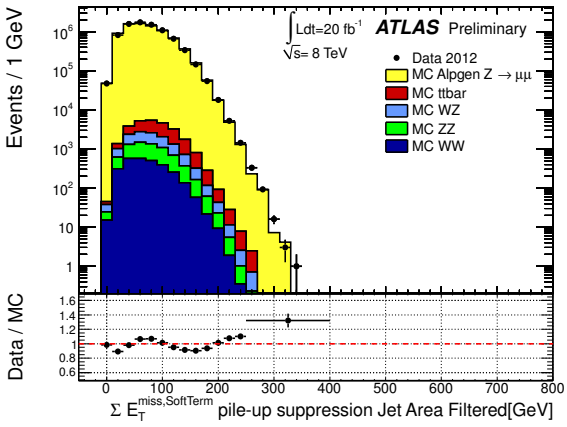

(d) pile-up suppression Jet Area Filtered

Figure 11: *Distribution of* $\sum E_T^{SoftTerm}$ *before pile-up suppression (a), corrected with STVF (b), corrected with Extrapolated Jet Area Filtered (c) and corrected with Jet Area Filtered (d) for* $Z \rightarrow \mu\mu$ *data. The expectation from Monte Carlo simulation (*ALPGEN*) is superimposed and normalized to data, after each MC sample is weighted with its corresponding cross-section. The lower parts of the figures show the ratio of data over MC.*

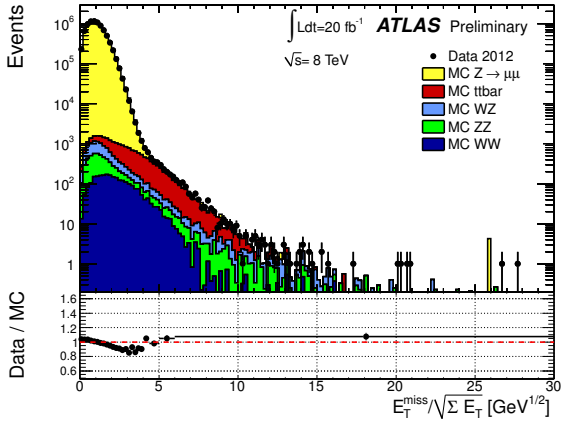

(a) before pile-up suppression

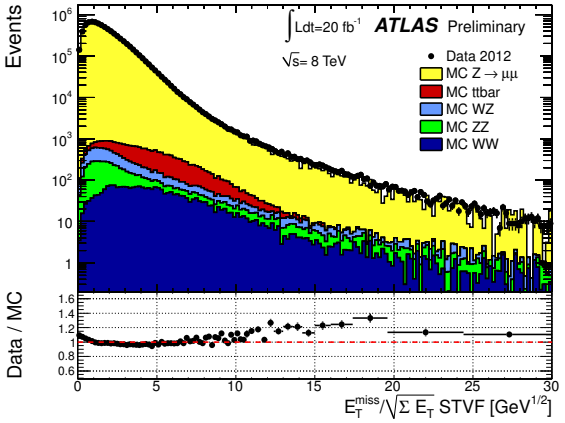

(b) after pile-up suppression with STVF

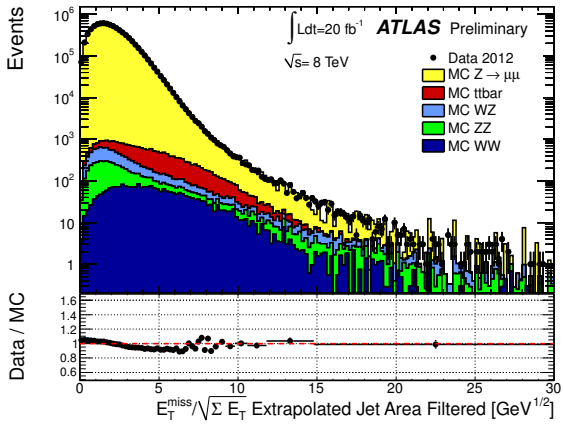

(c) pile-up suppression Extrapolated Jet Area Filtered

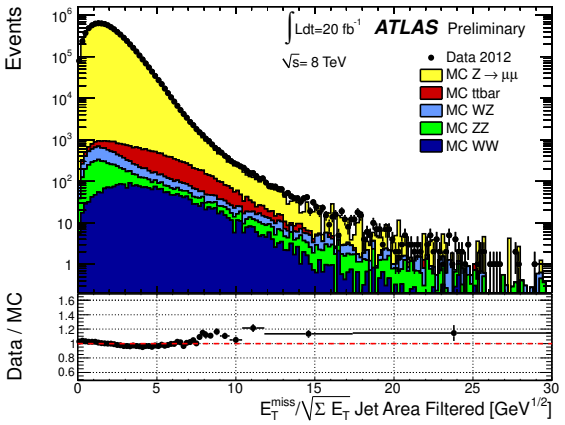

(d) pile-up suppression Jet Area Filtered

Figure 12: *Distributions of the ratio $E_T^{miss}/\sqrt{\Sigma E_T}$ in $Z \to \mu\mu$ data before (a) and after pile-up suppression with STVF (b), Extrapolated Jet Area Filtered (c) and Jet Area Filtered (d) pile-up suppression methods. The expectation from Monte Carlo simulation is superimposed and normalized to data, after each MC sample is weighted with its corresponding cross-section. The lower parts of the figures show the ratio of data over MC.*

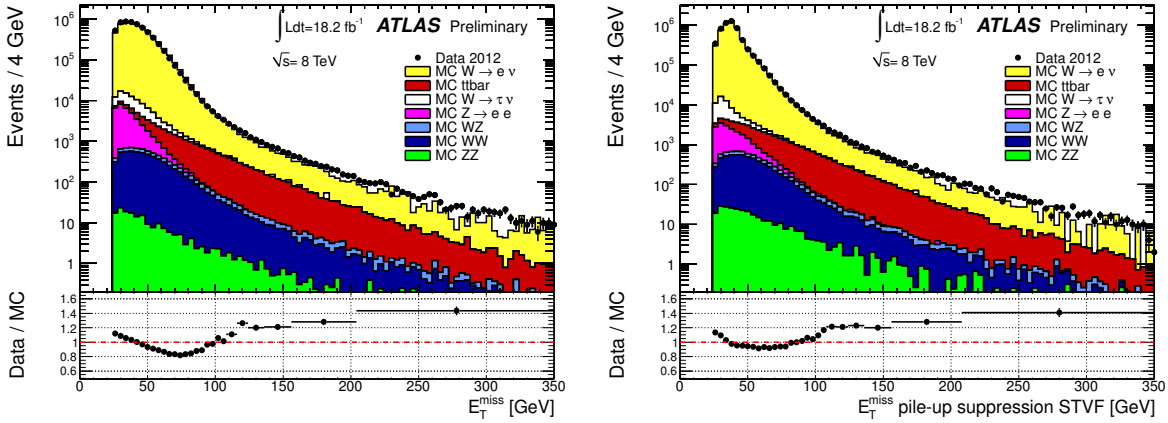

(a) before pile-up suppression

(b) after pile-up suppression with STVF

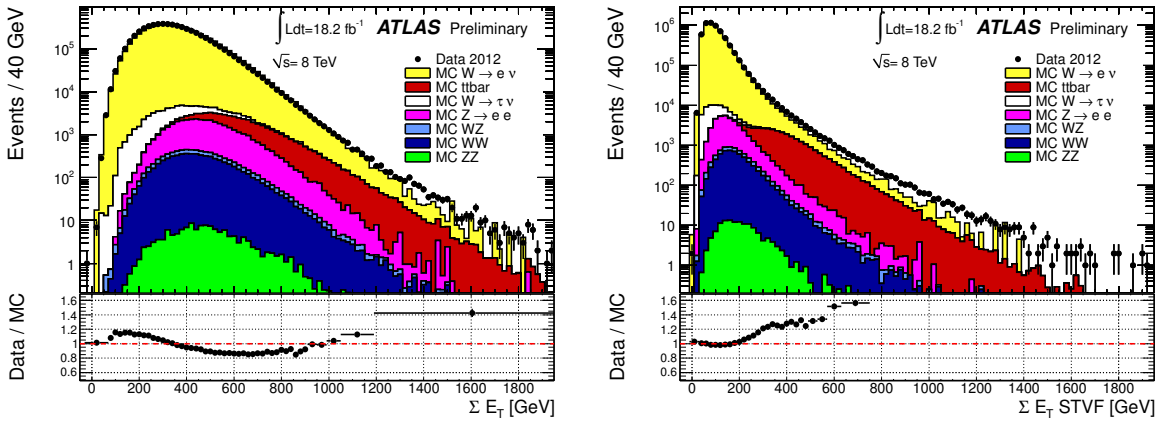

(c) before pile-up suppression

(d) after pile-up suppression with STVF

Figure 13: *Distribution of E_T^{miss} before (a) and after pile-up suppression with STVF (b) and distribution of $\sum E_T$ before (c) and after pile-up suppression with STVF (d), as measured in a data sample of $W \rightarrow e\nu$ events. The expectation from Monte Carlo simulation is superimposed and normalized to data, after each MC sample is weighted with its corresponding cross-section. The lower parts of the figures show the ratio of data over MC.*

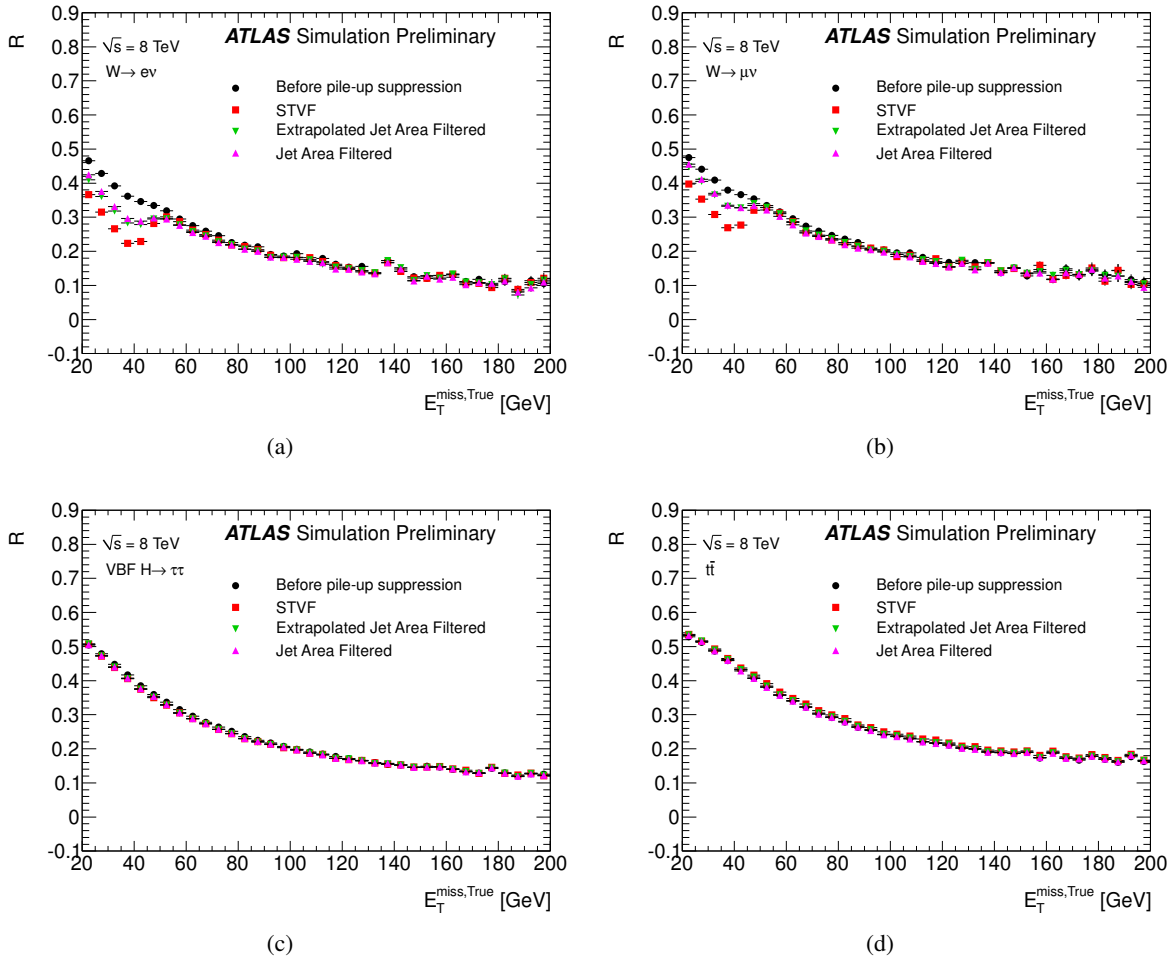

Figure 14: *Distribution of the ratio* $R = RMS(E_T^{miss}/E_T^{miss,True})/\langle E_T^{miss}/E_T^{miss,True}\rangle$ *as a function of* $E_T^{miss,True}$ *in MC* $W \to e\nu$ *(a),* $W \to \mu\nu$ *(b), VBF* $H \to \tau\tau$ *(c) and* $t\bar{t}$ *(d) events.*

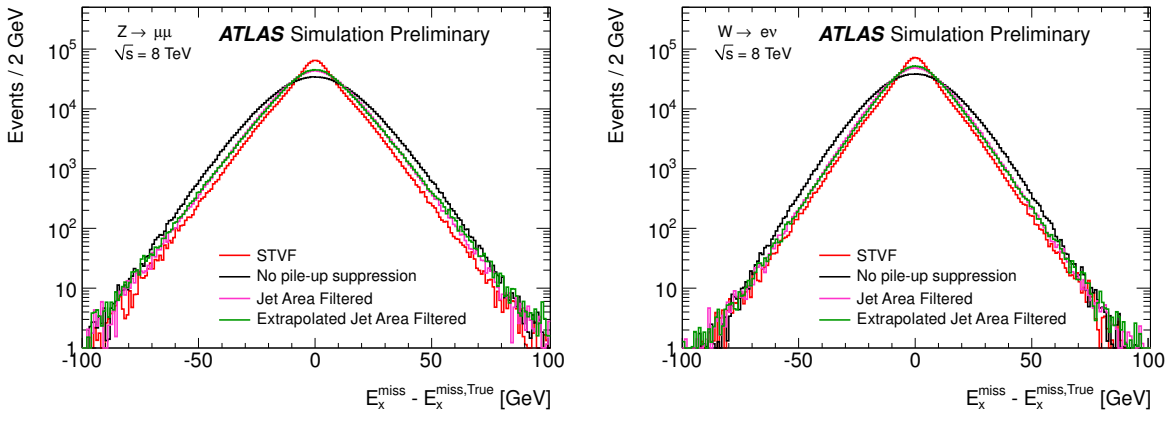

Figure 15: E_x^{miss} -$E_x^{miss,True}$ *distribution in MC* $Z \to \mu\mu$ *(a) and* $W \to e\nu$ *events (b).*

$\boldsymbol{E}_{\mathrm{T}}^{\mathrm{miss}}$ components, as defined above, in bins of the total transverse energy in the event, calculated from Equation 3. Both the E_x^{miss} and E_y^{miss} resolutions, which are very similar, are plotted for each event in Figures 16 - 18, so each distribution contains two entries per event. The core of each distribution is fitted, for each $\sum E_{\mathrm{T}}$ bin, with a Gaussian over a range spanning twice the expected resolution obtained in previous studies [1] and the fitted width, σ, is examined as a function of $\sum E_{\mathrm{T}}$ (event). As seen in Figure 15 for E_x^{miss} -$E_x^{\mathrm{miss,True}}$, the distributions are no longer Gaussian after pile-up suppression because of the different pile-up suppression in the jet term and in the soft term. In that case the quality of the Gaussian fit is good only when limiting the range of the fit to the core. Using the *RMS* instead would give similar results for the $\boldsymbol{E}_{\mathrm{T}}^{\mathrm{miss}}$ not corrected for the pile-up, while the results are worse by about 15(25)% after pile-up suppression with Jet Area (STVF) methods.

Figure 16 shows the resolution from data for minimum bias as a function of $\sum E_{\mathrm{T}}$ (event), before and after pile-up suppression with all the methods described in Section 6.

Figure 17 shows the resolution for $Z \to \ell\ell$ events from data as a function of $\sum E_{\mathrm{T}}$ (event), before and after pile-up suppression. In the same figure, the resolution in data and MC simulation is compared for $Z \to \ell\ell$ events showing that there is an excellent agreement between the resolutions in data and MC simulation both before and after pile-up suppression and the resolutions are very similar for the electron and muon channels.

In Figure 18 the $\boldsymbol{E}_{\mathrm{T}}^{\mathrm{miss}}$ resolution is shown for MC events for different processes with genuine $\boldsymbol{E}_{\mathrm{T}}^{\mathrm{miss}}$ as a function of $\sum E_{\mathrm{T}}$ (event). The lower x-axis shows the mean value of the $\sum E_{\mathrm{T}}^{\mathrm{SoftTerm}}$ for each $\sum E_{\mathrm{T}}$ (event) bin. A strong improvement of the resolution is achieved after pile-up suppression, in particular with the STVF method, in $Z \to \ell\ell$, $W \to \ell\nu$ events, where such improvement is less evident in the region with $E_{\mathrm{T}}^{\mathrm{miss}}$ larger than 600 GeV, populated by events with jets. The improvement in the resolution after pile-up suppression is smaller in VBF $H \to \tau\tau$ events because of the high jet activity in this topology that makes the correction on the soft term less significant. In $t\bar{t}$ and SUSY events, where the contribution to $\boldsymbol{E}_{\mathrm{T}}^{\mathrm{miss}}$ from the soft term is smaller (see the lower x-axis and Figure 2), there is no improvement in the resolution after pile-up suppression with any method. In particular, for SUSY events the best resolution is achieved with the $\boldsymbol{E}_{\mathrm{T}}^{\mathrm{miss}}$ without pile-up suppression, probably because in these events with a large number of jets, removing one jet or/and reducing the soft term can create an imbalance.

Figure 19 directly compares the resolution in all MC samples considered and shows that the resolution is similar for all samples before pile-up suppression, while it is clear that the effect of the pile-up suppression on the resolution is very dependent on the contribution of the soft term that is different for different topologies. In particular the pile-up suppression is more effective for the topologies with higher fractional contribution of the soft term (like Z and W events), see Figure 2 and 18, than those with a lower fractional contribution from the soft term like $t\bar{t}$ or SUSY.

7.4 $\boldsymbol{E}_{\mathrm{T}}^{\mathrm{miss}}$ response

It is important to check that the pile-up suppression methods, introduced to reduce the effect of pile-up on the MET resolution, do not have an adverse affect on the MET response.

The $\boldsymbol{E}_{\mathrm{T}}^{\mathrm{miss}}$ response has been checked in many ways. The first is in $Z \to \ell\ell$ events, in which the projection of the $\boldsymbol{E}_{\mathrm{T}}^{\mathrm{miss}}$ along the transverse direction of the Z boson, for different values of the Z boson p_{T}, is considered. The second is the study of the $\boldsymbol{E}_{\mathrm{T}}^{\mathrm{miss}}$ linearity in MC events in different channels. Finally the $\boldsymbol{E}_{\mathrm{T}}^{\mathrm{miss}}$ response has been checked by considering the reconstructed mass in $W \to \ell\nu$, $Z \to \tau\tau$ and $H \to \tau\tau$ events, each of which contain true $\boldsymbol{E}_{\mathrm{T}}^{\mathrm{miss}}$ from unobserved neutrinos.

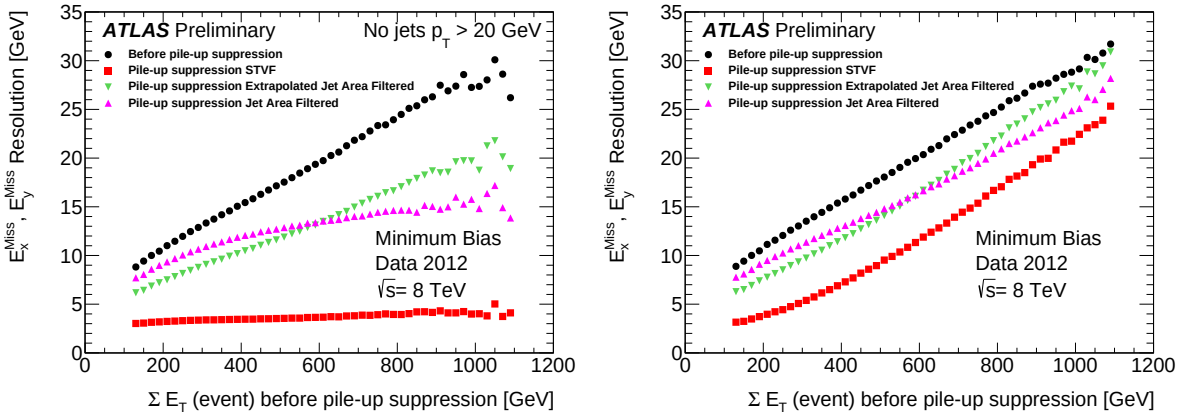

Figure 16: E_x^{miss} *and* E_y^{miss} *resolution as a function of the total transverse energy in the event calculated by summing the* p_T *of muons and the total transverse energy in the calorimeter in data. Results are shown before and after pile-up suppression with different methods for minimum bias events without jets with* $p_T > 20\,GeV$ *(a) and inclusive (b) 2012 data.*

7.4.1 Final states with no genuine $E_{\mathrm{T}}^{\mathrm{miss}}$: response in $Z \to \ell\ell$ events

From the event topology in events with $Z \to \ell\ell$ decays one can define an axis in the transverse plane such that the component of $\boldsymbol{E}_{\mathrm{T}}^{\mathrm{miss}}$ along this axis is sensitive to detector resolution and biases [30]. This axis, $\boldsymbol{A_Z}$, is defined by the reconstructed momenta of the leptons:

$$\boldsymbol{A_Z} = (\ \boldsymbol{p_T}^{\ell^+} + \ \boldsymbol{p_T}^{\ell^\pm})/|\,\boldsymbol{p_T}^{\ell^+} + \boldsymbol{p_T}^{\ell^-}|, \tag{7}$$

where $\boldsymbol{p_T}^{\ell}$ are the vector transverse momenta of the lepton and anti-lepton. The direction of $\boldsymbol{A_Z}$ thus reconstructs the transverse direction of motion of the Z boson.

The mean value of the projection of $\boldsymbol{E}_{\mathrm{T}}^{\mathrm{miss}}$ onto the longitudinal axis, $\langle \boldsymbol{E}_{\mathrm{T}}^{\mathrm{miss}} \cdot \boldsymbol{A_Z} \rangle$, is a test of the $\boldsymbol{E}_{\mathrm{T}}^{\mathrm{miss}}$ calculation, as this axis is sensitive to the balance between the leptons and the hadronic recoil. The study of the distribution of $\langle \boldsymbol{E}_{\mathrm{T}}^{\mathrm{miss}} \cdot \boldsymbol{A_Z} \rangle$, is also very useful to understand if the methods to suppress pile-up preserve the $\boldsymbol{E}_{\mathrm{T}}^{\mathrm{miss}}$ response.

Figure 20 shows the value of $\langle \boldsymbol{E}_{\mathrm{T}}^{\mathrm{miss}} \cdot \boldsymbol{A_Z} \rangle$ as a function of the Z tranverse momentum, p_{T}^{Z}. These mean values are used as a diagnostic tool to validate the $\boldsymbol{E}_{\mathrm{T}}^{\mathrm{miss}}$ reconstruction algorithms. If the leptons perfectly balanced the hadronic recoil, regardless of the net momentum of the lepton system, then the $\boldsymbol{E}_{\mathrm{T}}^{\mathrm{miss}} \cdot \boldsymbol{A_Z}$ would be zero, independent of p_{T}^{Z}. A negative bias is seen in both electron and muon channels of the same order of magnitude suggesting that an underestimation of the hadronic recoil is the source of the bias. In particular in the region of p_{T}^{Z} below $\sim 40\,\mathrm{GeV}$, dominated by events without jets, the bias is enhanced due the underestimation of $E_{\mathrm{T}}^{\mathrm{miss,SoftTerm}}$. After STVF pile-up suppression the bias is further increased suggesting that this method tends to over-suppress the soft term removing not only the pile-up but also some fraction of the hadronic recoil.

Figure 21 shows that there is a good agreement between the values of $\langle \boldsymbol{E}_{\mathrm{T}}^{\mathrm{miss}} \cdot \boldsymbol{A_Z} \rangle$ as a function of the Z tranverse momentum p_{T}^{Z} in data and MC simulation for $Z \to \mu\mu$ and $Z \to ee$. There is some disagreement between the electron and the muon channels, probably due to the fact that the parametrized energy loss of the muon in the calorimeter is subtracted from the muon momentum when the combined muon measurement is used (see Section 5). This correction can be overestimated if the energy deposited by the muon in the calorimeters is not enough to seed a topocluster.

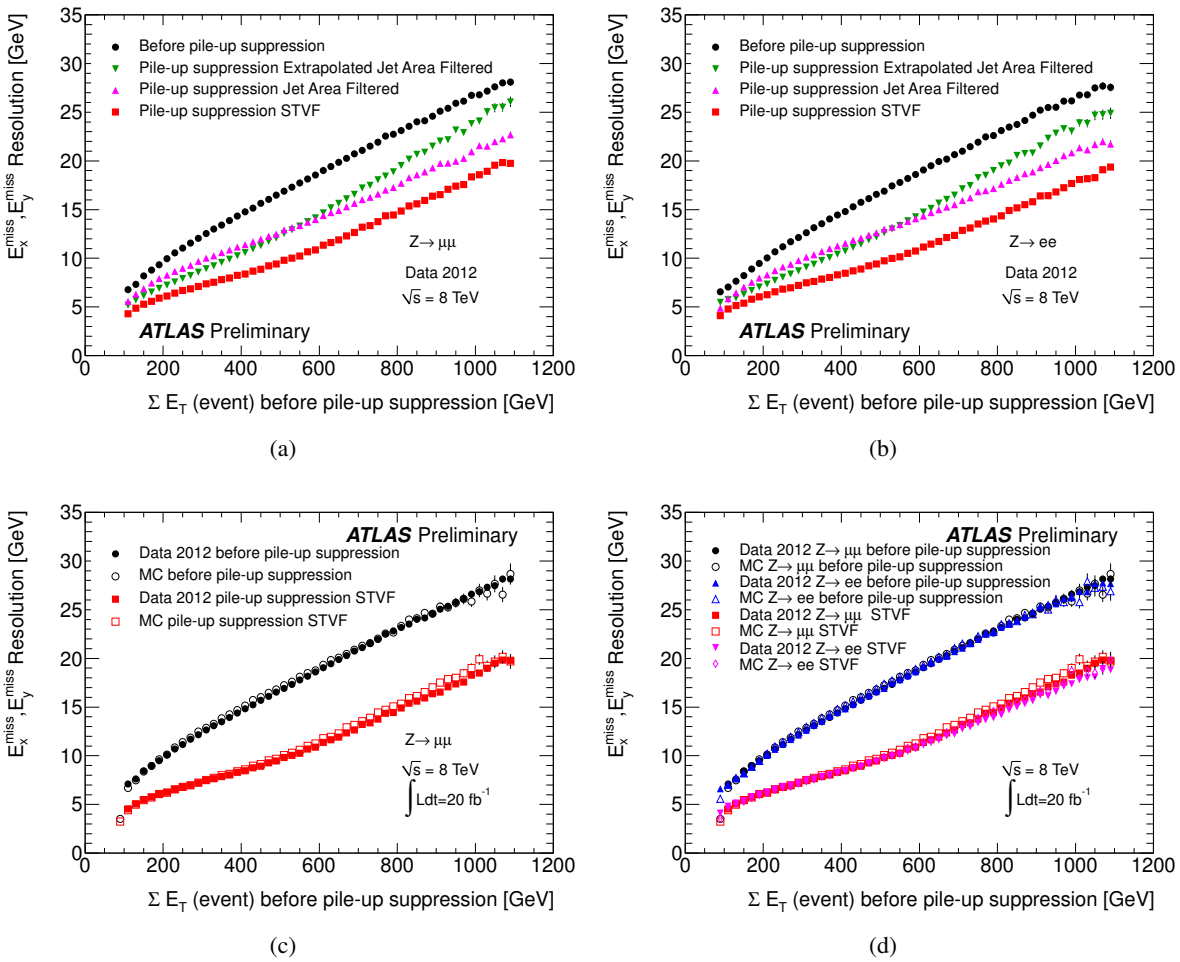

Figure 17: *E_x^{miss} and E_y^{miss} resolution as a function of the total transverse energy in the event calculated by summing the p_T of muons and the total transverse energy in the calorimeter in data. Results are shown for $Z \to \mu\mu$ (a) and $Z \to ee$ (b) events before and after pile-up suppression with different methods. Resolution in data and MC simulation are compared in $Z \to \mu\mu$ (c) and $Z \to \mu\mu$ and $Z \to ee$ events (d).*

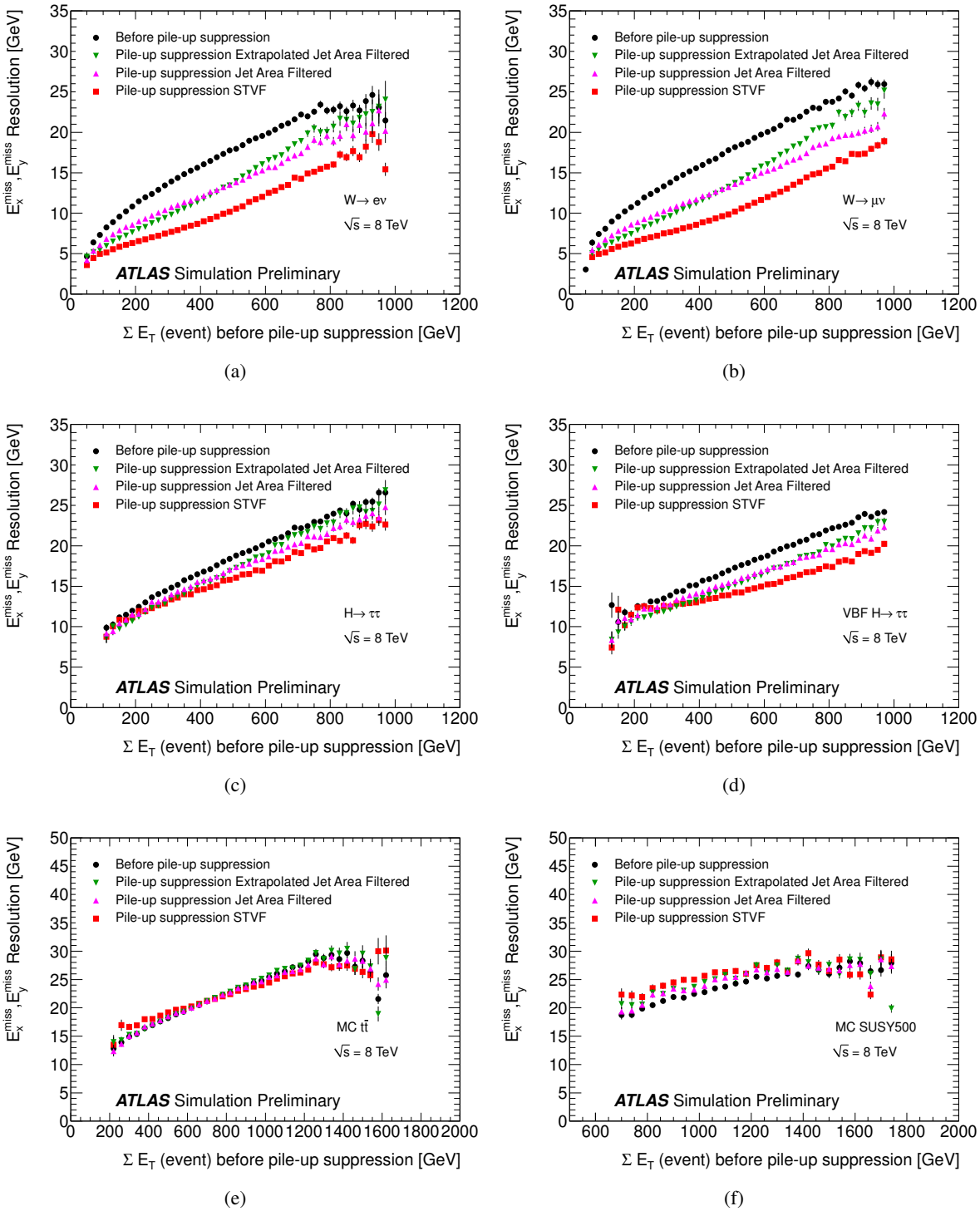

Figure 18: E_x^{miss} *and* E_y^{miss} *resolution as a function of the total transverse energy in the event calculated by summing the* p_T *of muons and the total transverse energy in the calorimeter in MC events. Results are shown before and after pile-up suppression with different methods for MC* $W \to e\nu$ *events (a),* $W \to \mu\nu$ *events (b),* $H \to \tau\tau$ $(m_H = 125\,GeV)$ *(c), VBF* $H \to \tau\tau$ $(m_H = 125\,GeV)$ *(d),* $t\bar{t}$ *(e), SUSY events (f).*

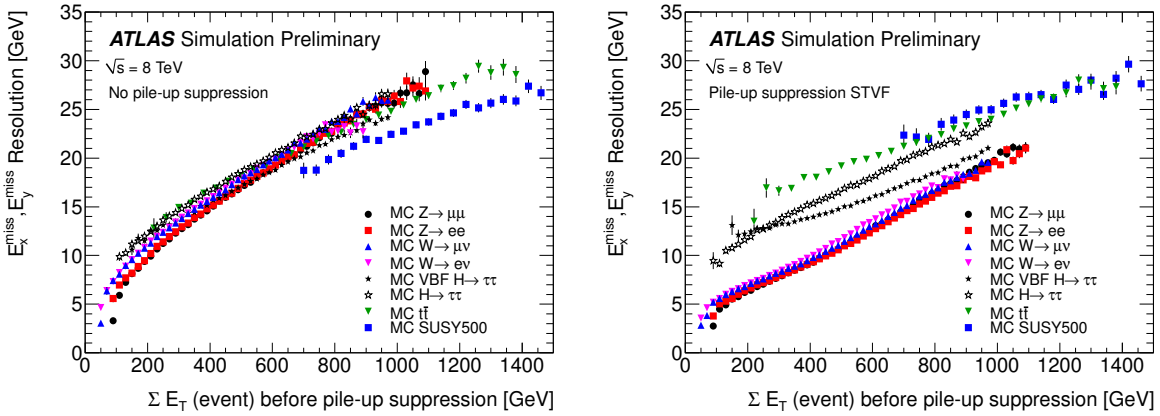

(a) (b)

Figure 19: E_x^{miss} *and* E_y^{miss} *resolution: summary plots comparing all MC samples before pile-up suppression (a) and after pile-up suppression with STVF (b).*

An evaluation of the $\boldsymbol{E}_{\mathrm{T}}^{\mathrm{miss}}$ scale can be provided by the distribution of the hadronic recoil in $Z \to \ell\ell$ events, defined as the vectorial difference of $\boldsymbol{E}_{\mathrm{T}}^{\mathrm{miss}}$ and $\mathbf{p}_{\mathrm{T}}^{Z}$. Figure 22 shows the value of the hadronic recoil, projected onto $\mathbf{p}_{\mathrm{T}}^{Z}$ and divided by p_{T}^{Z}, as a function of p_{T}^{Z} in $Z \to \ell\ell$ events. For low values of p_{T}^{Z}, the hadronic recoil is underestimated in a similar way in $Z \to \mu\mu$ and $Z \to ee$, leading to the same conclusions as for Figures 20 and 21.

Figure 23 shows that the cost of improving the resolution seems to be that the pile-up suppression procedure tends to artificially reduce that part of the soft term which should balance the Z boson p_{T} in $Z \to \mu\mu$ events. In fact, after pile-up suppression with the STVF method, a strong correlation between $\boldsymbol{E}_{\mathrm{T}}^{\mathrm{miss}}$ and p_{T}^{Z} is observed in events without jets suggesting once more that the STVF method tends to over-suppress the soft term, removing not only the pile-up but also some fraction of the hadronic recoil.

7.4.2 Final states with genuine $\boldsymbol{E}_{\mathrm{T}}^{\mathrm{miss}}$: linearity and azimuthal direction measurement

- $\boldsymbol{E}_{\mathrm{T}}^{\mathrm{miss}}$ linearity

The $E_{\mathrm{T}}^{\mathrm{miss}}$ linearity is defined as the mean value of the ratio: $(E_{\mathrm{T}}^{\mathrm{miss}} - E_{\mathrm{T}}^{\mathrm{miss,True}})/E_{\mathrm{T}}^{\mathrm{miss,True}}$. The mean value of this ratio is expected to be zero if $E_{\mathrm{T}}^{\mathrm{miss}}$ is reconstructed at the correct scale. The linearity for the different MC samples considered is shown in Figure 24. For all the samples a positive bias is observed for low $E_{\mathrm{T}}^{\mathrm{miss,True}}$ values which is due to the finite resolution of the $\boldsymbol{E}_{\mathrm{T}}^{\mathrm{miss}}$ measurement. For larger $E_{\mathrm{T}}^{\mathrm{miss,True}}$ values, the bias is within 5% for all samples. Differences in the linearity before and after pile-up suppression are visible, except for SUSY events where the linearity is good and not affected by the pile-up suppression. In particular in $W \to \ell\nu$ events, a larger non-linearity is observed for STVF, because of the strong pile-up suppression mainly in events without jets. In any case, the bulk of the events have a $E_T^{\mathrm{miss,True}}$ between about 35 and 40 GeV, where the linearity for STVF is within 7%. The linearity is improved in $H \to \tau\tau$ (VBF $H \to \tau\tau$) events after pile-up suppression in the region around the average $E_T^{\mathrm{miss,True}}$ of 40 (50) GeV. The linearity is stable after pile-suppression with STVF, while it seems slightly worse after pile-up suppression with the jet area methods in the region of the average $E_T^{\mathrm{miss,True}}$ of 70 GeV, for $t\bar{t}$ events.

Figure 25 directly compares the linearity in all MC samples considered and shows that the linearity is similar for all samples and within 5% for all samples, while there is a larger bias in $W \to \ell\nu$ events

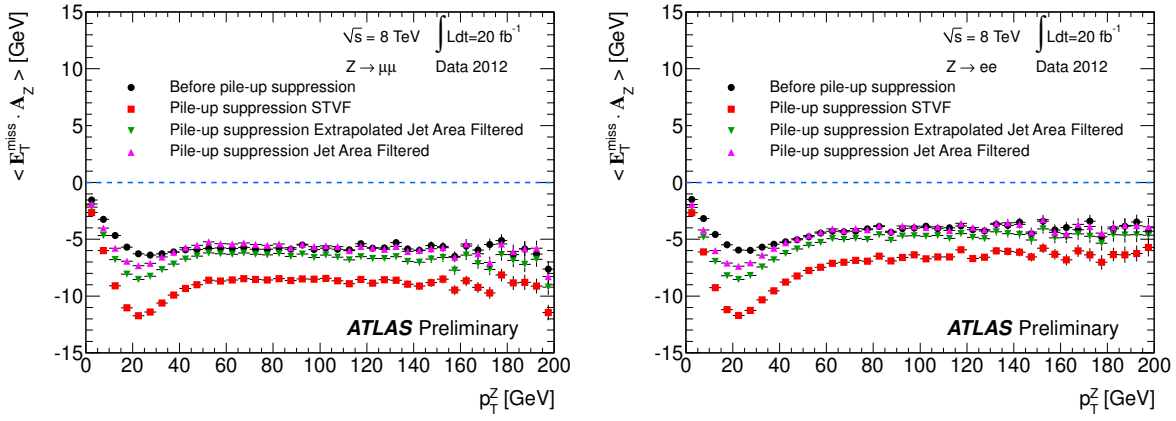

(a) (b)

Figure 20: *Mean values of the projection of $\boldsymbol{E}_T^{miss}$ onto the direction of the Z boson as a function of the transverse momentum of the Z boson in $Z \to \mu\mu$ data (a) and $Z \to ee$ data (b) before and after pile-up suppression with different methods.*

and $H \to \tau\tau$ events for low $E_T^{\text{miss,True}}$ values, due to the strong pile-up suppression using STVF in events without jets.

- $\boldsymbol{E}_{\text{T}}^{\text{miss}}$ azimuthal direction measurement

The ϕ^{miss} measurement is affected by pile-up, so it is important to check how ϕ^{miss} is improved after pile-up suppression.

After the pile-up suppression, the width of the distribution of the difference of the reconstructed and true ϕ^{miss} is more stable as a function of N_{pv}. Figure 26 shows the width of the distribution of the difference of the reconstructed and true ϕ^{miss} as a function of the true $\boldsymbol{E}_{\text{T}}^{\text{miss}}$. The ϕ^{miss} measurement improves when the true $\boldsymbol{E}_{\text{T}}^{\text{miss}}$ increases, as expected.

7.5 Reconstruction of mass in final states with neutrinos

7.5.1 $W \to \ell\nu$ events: transverse mass reconstruction

The reconstructed transverse mass, m_{T}, of the $\mathbf{p}_{\text{T}}$ lepton and $\boldsymbol{E}_{\text{T}}^{\text{miss}}$ system, defined in Section 3.3, is sensitive both to the scale and the resolution of $\boldsymbol{E}_{\text{T}}^{\text{miss}}$.

Figure 27 shows that the $E_{\text{T}}^{\text{miss}}$ is closer to $E_T^{\text{miss,True}}$ after the pile-up suppression, and that m_{T} is also improved. The improvement in m_{T} is less evident because both the $E_{\text{T}}^{\text{miss}}$ value and direction enter in the m_{T} reconstruction.

Figure 28 shows how well the m_{T} is reconstructed with respect to the true m_{T} value as a function of the m_{T} true itself and of $E_T^{\text{miss,True}}$. As shown in Figures 14 and 24, for $W \to \ell\nu$ events, for values of $E_T^{\text{miss,True}}$ between about 35 and 40 GeV, where the majority of the events belong, the scale of the reconstructed $\boldsymbol{E}_{\text{T}}^{\text{miss}}$ shows small differences depending on whether pile-up suppression is used or not and it is very close to the $E_T^{\text{miss,True}}$. What is important to note is that the resolution in the pile-up suppressed case is much better (by about 30%) with respect to the non pile-up suppressed case as clearly shown in Figure 27 (a). The reconstructed m_{T} in W events is thus marginally improved by the usage of a pile-up suppression technique, and, as shown in Figure 27 (b), the resolution improvement allows for a better estimation of m_{T}.

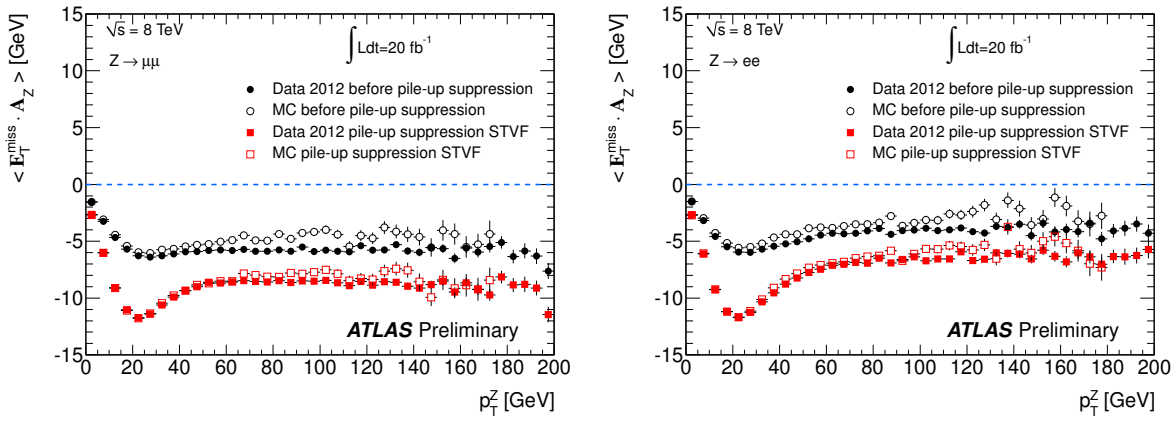

(a) (b)

Figure 21: *Mean values of the projection of $\boldsymbol{E}_T^{miss}$ onto the direction of the Z boson as a function of the transverse momentum of the Z boson in $Z \to \mu\mu$ data and MC (a) and $Z \to ee$ data and MC events (b) before and after pile-up suppression with the STVF method.*

7.5.2 $Z \to \tau\tau$ and $H \to \tau\tau$ MC events: invariant mass reconstruction

A very good measurement of the $\boldsymbol{E}_{\mathrm{T}}^{\mathrm{miss}}$ is fundamental for the study of these channels because the $\boldsymbol{E}_{\mathrm{T}}^{\mathrm{miss}}$ components are ingredients for the $\tau\tau$ invariant mass reconstruction. The $\tau\tau$ mass can be reconstructed with the collinear approximation or using the Missing Mass Calculator method (MMC) [31]. The invariant mass reconstructed with the collinear approximation [30] is used in the following because it is more sensitive to $\boldsymbol{E}_{\mathrm{T}}^{\mathrm{miss}}$ performance than the MMC is. In fact, the width of the reconstructed $m_{\tau\tau}$ is completely dominated by the $\boldsymbol{E}_{\mathrm{T}}^{\mathrm{miss}}$ resolution and its peak position depends on the $\boldsymbol{E}_{\mathrm{T}}^{\mathrm{miss}}$ scale. The improvement of $\boldsymbol{E}_{\mathrm{T}}^{\mathrm{miss}}$ resolution with pile-up suppression is crucial for Higgs searches in the decay channel to a pair of taus.

Results are shown here for the lepton-hadron channel, where one τ decays to a lepton (electron or muon) and the other to hadrons. The invariant $m_{\tau\tau}$ is reconstructed for events with one identified τ-jet with $p_{\mathrm{T}} > 20\,\mathrm{GeV}$ and one identified lepton with $p_{\mathrm{T}} > 20\,\mathrm{GeV}$ and with an opening angle between the τ-jet and the lepton between 0.5 and 2.9 rad. Figure 29 shows the reconstructed $m_{\tau\tau}$ in lepton-hadron MC $Z \to \tau\tau$ and VBF $H \to \tau\tau$ (with m_H=125 GeV) events without pile-up suppression and after pile-up suppression with the different methods described in Section 6. All histograms are normalized to the number of events in which the invariant mass before pile-up suppression can be reconstructed. The figure shows that the $m_{\tau\tau}$ reconstructed with the collinear approximation has a narrower distribution when $\boldsymbol{E}_{\mathrm{T}}^{\mathrm{miss}}$ with pile-up suppression is used. This is particularly true when the STVF $\boldsymbol{E}_{\mathrm{T}}^{\mathrm{miss}}$ is used. The narrower resolution achieved after pile-up suppression improves the separation between $Z \to \tau\tau$ and $H \to \tau\tau$, enhancing the ability to identify $H \to \tau\tau$ events.

Another important aspect in the invariant mass reconstruction with the collinear approximation is the mass reconstruction efficiency. Efficiency (defined as the the fraction of events where the invariant mass in the collinear approximation can be reconstructed) is lost if the mass cannot be reconstructed due to the two τ-leptons being back-to-back or when the $\boldsymbol{E}_{\mathrm{T}}^{\mathrm{miss}}$ measurement (magnitude and direction) is poor. In VBF $H \to \tau\tau$ ($Z \to \tau\tau$) events, the mass reconstruction efficiency decreases from 97(93)% when using the $E_T^{\mathrm{miss,True}}$ to 80(65)% when using the reconstructed $\boldsymbol{E}_{\mathrm{T}}^{\mathrm{miss}}$ before pile-up suppression. It is $\sim$ 80(55)% when using the $\boldsymbol{E}_{\mathrm{T}}^{\mathrm{miss}}$ after pile-up suppression with STVF and $\sim$ 80(60)% when using the Jet Area pile-up suppression. The efficiency of the $Z \to \tau\tau$ mass reconstruction is smaller even using

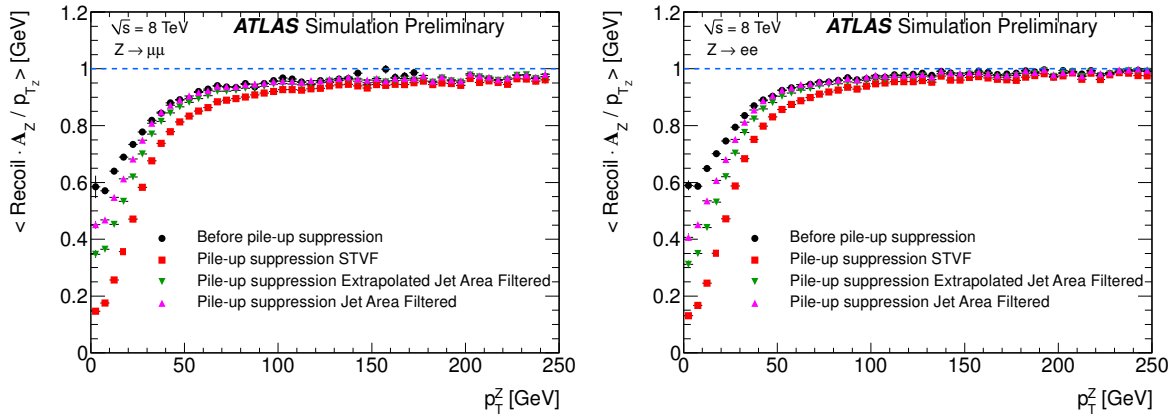

(a) (b)

Figure 22: *Hadronic recoil, defined as the vectorial difference of $\boldsymbol{E}_T^{miss}$ and $\boldsymbol{p}_T^Z$, projected onto $\boldsymbol{p}_T^Z$ and divided by p_T^Z, for $Z \to \mu\mu$ (a) and $Z \to ee$ (b) simulated events as a function of p_T^Z.*

the $E_T^{\text{miss,True}}$ because the two τ-leptons are more back-to-back (the Z is less boosted than the H produced through VBF) and when using the $\boldsymbol{E}_{\text{T}}^{\text{miss}}$ before pile-up suppression because the $Z \to \tau\tau$ events have a smaller $E_{\text{T}}^{\text{miss}}$. It decreases after the pile-up suppression because the $E_{\text{T}}^{\text{miss}}$ becomes very small, mainly in the events with no jets, so the probability to have a negative solution for for one or both neutrino momenta increases. These differences in the reconstruction efficiency after the pile-up suppression in the two samples improve the signal significance.

7.6 Study of tails in $\boldsymbol{E}_{\text{T}}^{\text{miss}}$ distribution

The tails of the $E_{\text{T}}^{\text{miss}}$ distribution can lead to an additional background in searches for new undetected particles. It is important that the methods used to narrow the bulk of the resolution function do not increase the size of those tails. Figure 30 compares the number of events which have $E_{\text{T}}^{\text{miss}}$ above a fixed threshold before and after the pile-up suppression with the various methods considered in this note for MC events in different samples. It can be seen that the pile-up mitigation techniques do not significantly increase the tails of the MET resolution functions. Few additional tails are created in events with jets after pile-up suppression and they are similar for all the pile-up suppression methods, while no tails are observed in events with no jets.

8 Evaluation of the systematic uncertainty on $\boldsymbol{E}_{\text{T}}^{\text{miss}}$

The $\boldsymbol{E}_{\text{T}}^{\text{miss}}$, as defined in Section 5, is the sum of several terms corresponding to different types of reconstructed objects. The uncertainty on each individual term is evaluated given the knowledge of the reconstructed objects that are used to build it. The overall systematic uncertainty on the $E_{\text{T}}^{\text{miss}}$ measurement is then calculated by combining the uncertainties on each term.

The relative impact of the uncertainty of the constituent terms on $E_{\text{T}}^{\text{miss}}$ depends on the event topology. In particular, in events containing W and Z bosons decaying to leptons, uncertainties on the scale and resolution of the charged leptons, together with uncertainties on the jet energy scale and resolution, need to be propagated to the systematic uncertainty estimate for $E_{\text{T}}^{\text{miss}}$. Another significant contribution

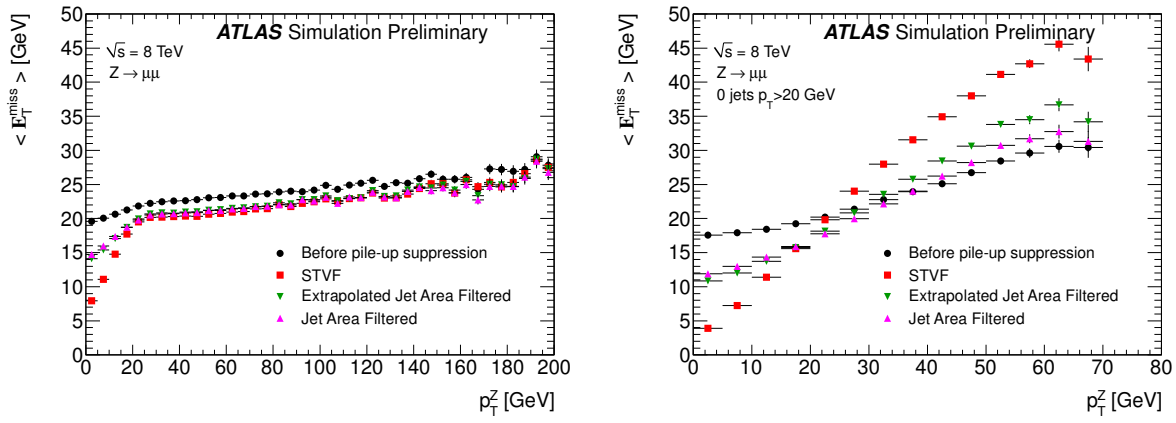

(a) (b)

Figure 23: *Mean values of $\boldsymbol{E}_T^{miss}$ as a function of the transverse momentum of the Z boson in $Z \to \mu\mu$ events, inclusive events (a) and in events without jets (b).*

to the $E_{\mathrm{T}}^{\mathrm{miss}}$ uncertainty in W and Z boson final states comes from the soft contributions. This soft term has a smaller impact in other channels, as can be seen from Figure 2.

Two methods for the evaluation of the systematic uncertainty on the scale and on the resolution of the $E_{\mathrm{T}}^{\mathrm{miss,SoftTerm}}$, which arises from both the MC modeling and the effects of pile-up, have been developed and are extensively documented in Ref. [2]. The methods have been applied to quantify the systematic uncertainty on the scale and on the resolution of the $E_{\mathrm{T}}^{\mathrm{miss,SoftTerm}}$ in 8 TeV samples using $Z \to \mu\mu$ events, selected as described in Section 3.2. In the following the methods are briefly described and the uncertainties obtained for $E_{\mathrm{T}}^{\mathrm{miss,SoftTerm}}$ before and after pile-up suppressions are shown together with the closure tests.

8.1 Evaluation from data/MC ratio in events without jets

The subset of $Z \to \mu\mu$ events that do not contain jets with $p_{\mathrm{T}} > 20\,\mathrm{GeV}$ is selected because in these events only the leptons and the soft term contribute to $\boldsymbol{E}_{\mathrm{T}}^{\mathrm{miss}}$. The systematic uncertainty on the soft term scale and resolution is determined from the comparison of observables in data with the Monte Carlo prediction for events without jets.

The projection of the $\boldsymbol{E}_{\mathrm{T}}^{\mathrm{miss}}$ onto the Z boson transverse direction provides a test of possible bias on the $\boldsymbol{E}_{\mathrm{T}}^{\mathrm{miss}}$ scale. The data-MC ratio of this observable in $Z \to \mu\mu$ events without jets is used as a measure of the systematic uncertainty on the scale of the soft term, which is calculated as the average deviation from unity. The systematic uncertainty on the soft term resolution is determined in a similar manner, this time using the E_x^{miss} and E_y^{miss} resolution to quantify the level of agreement.

The events simulated with POWHEG + PYTHIA8 were used to determine the systematic uncertainties on the soft term with this method. It has also been checked that these uncertainties cover the data-MC discrepancies when using $Z \to \mu\mu$ events generated with ALPGEN.

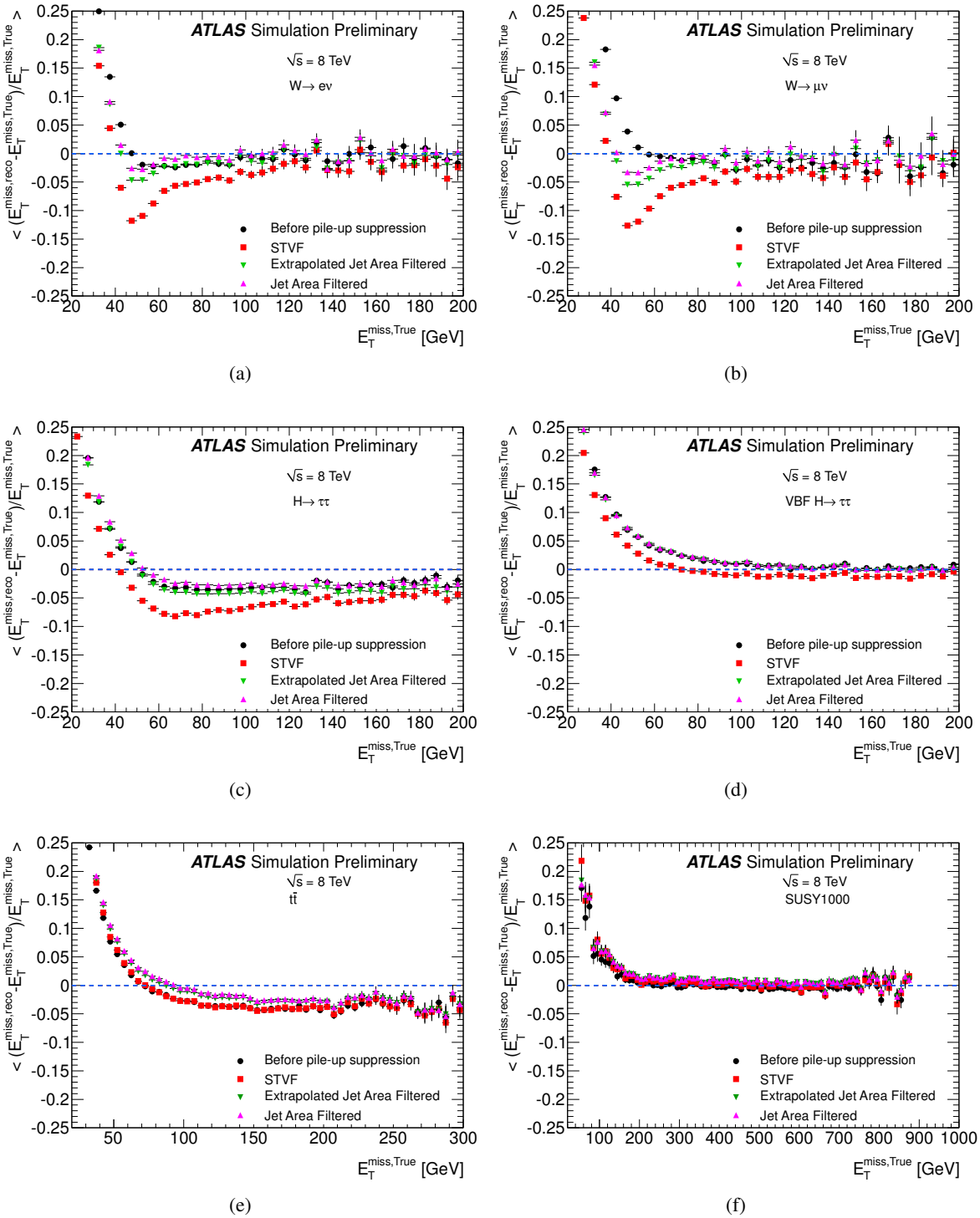

Figure 24: E_T^{miss} *linearity in* $W \rightarrow e\nu$ *(a),* $W \rightarrow \mu\nu$ *(b),* $H \rightarrow \tau\tau$ $(m_H = 125\,GeV)$ *(c), VBF* $H \rightarrow \tau\tau$ $(m_H = 125\,GeV)$ *(d),* $t\bar{t}$ *(e) and SUSY (f) MC events as a function of the true* E_T^{miss}.

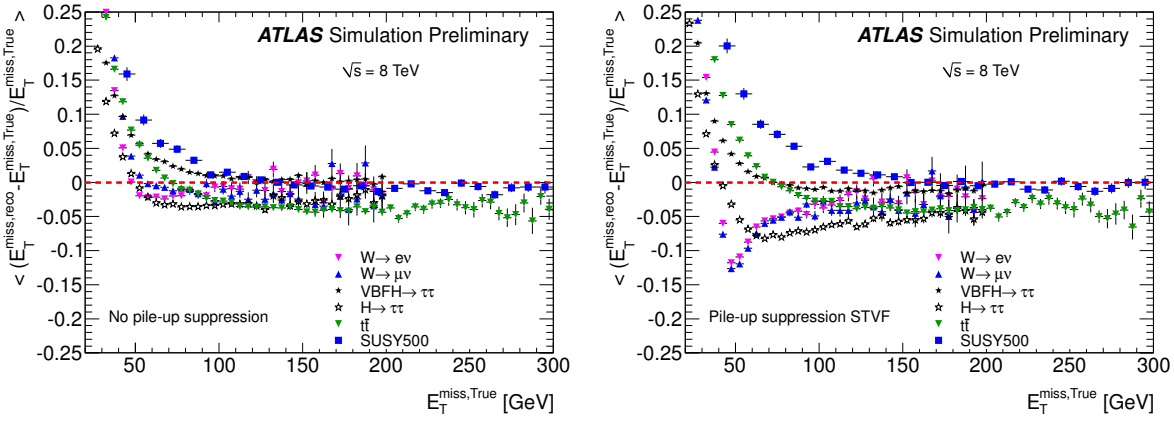

(a) (b)

Figure 25: *Linearity: summary plots comparing MC samples before pile-up suppression (a) and after pile-up suppression with STVF (b)* .

8.2 Evaluation from the balance between soft terms and hard objects

This method uses inclusive $Z \rightarrow \mu\mu$ events and exploits the balance between the $E_{\mathrm{T}}^{\mathrm{miss,SoftTerm}}$ and the total transverse momentum of the hard objects in the events, defined as:

$$\begin{aligned} p_{x(y)}^{\mathrm{hard}} &= \Sigma_{\mu}\, p_{x(y)}^{\mu} + \Sigma_{\mathrm{e}}\, p_{x(y)}^{\mathrm{e}} + \Sigma_{\mathrm{jets}}\, p_{x(y)}^{\mathrm{jets}} + \Sigma_{\gamma}\, p_{x(y)}^{\gamma} + \Sigma_{\nu}\, p_{x(y)}^{\nu}, \\ p_{\mathrm{T}}^{\mathrm{hard}} &= \sqrt{(p_x^{\mathrm{hard}})^2 + (p_y^{\mathrm{hard}})^2}. \end{aligned} \tag{8}$$

$p_{\mathrm{x(y)}}^{\mathrm{hard}}$ is in general calculable only for MC events, since it includes invisible particle momenta which are not known in data. While not an observable, it is nevertheless a useful quantity to characterise events since transverse momentum balance dictates that it ought to be equal to $E_{x(y)}^{\mathrm{miss,SoftTerm}}$.

The mean and the resolution of the $\boldsymbol{E}_{\mathrm{T}}^{\mathrm{miss,SoftTerm}}$ components have been studied both with respect to $p_{\mathrm{T}}^{\mathrm{hard}}$ and to N_{pv} to study the effect of pile-up. In these events $p_{x(y)}^{\nu}$ is close to zero and it is assumed to be zero in data. Since the magnitude and direction of the $\boldsymbol{E}_{\mathrm{T}}^{\mathrm{miss,SoftTerm}}$ depends on the number of jets, leptons and neutrinos in the event, the systematic uncertainties have been derived in bins of $p_{x(y)}^{\mathrm{hard}}$. Therefore the parametrization determined from $Z \rightarrow \mu\mu$ events can be used to evaluate the systematic uncertainties on the $E_{\mathrm{T}}^{\mathrm{miss,SoftTerm}}$ in other samples as well. It should be noted that this method makes use of the neutrino information, so it can be applied only in MC simulation.

To evaluate the $\boldsymbol{E}_{\mathrm{T}}^{\mathrm{miss,SoftTerm}}$ mean and resolution, the $\boldsymbol{E}_{\mathrm{T}}^{\mathrm{miss,SoftTerm}}$ is decomposed along the $p_{\mathrm{T}}^{\mathrm{hard}}$ direction and along the orthogonal direction, referred to as longitudinal (L) and perpendicular (P) directions, respectively. The mean longitudinal component is a measure of the $\boldsymbol{E}_{\mathrm{T}}^{\mathrm{miss,SoftTerm}}$ scale, as the longitudinal direction is sensitive to the balance between the high-p_{T} objects and the $\boldsymbol{E}_{\mathrm{T}}^{\mathrm{miss,SoftTerm}}$.

8.3 Scale and resolution uncertainty of soft term and closure tests

Table 1 shows the uncertainties on the $\boldsymbol{E}_{\mathrm{T}}^{\mathrm{miss,SoftTerm}}$ scale and resolution calculated with the two methods described above, before and after pile-up suppression using STVF or jet area as explained in Section 6.

Figure 31 shows the closure test for the systematic uncertainties, calculated with the data/MC ratio method, in $Z \rightarrow \mu\mu$ events without jets. In these events the $\boldsymbol{E}_{\mathrm{T}}^{\mathrm{miss}}$ is built only from the muon term

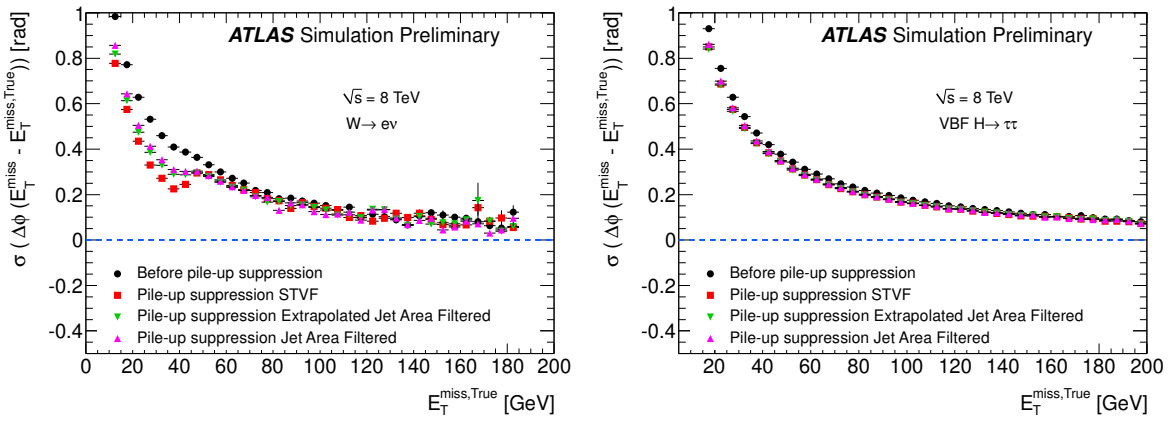

(a) (b)

Figure 26: *Width of the difference of the reconstructed and true ϕ^{miss} as a function of the true E_T^{miss} in $W \to e\nu$ events (a) and in VBF $H \to \tau\tau$ events (b). The default $\boldsymbol{E}_T^{miss}$ is compared with the $\boldsymbol{E}_T^{miss}$ after the pile-up correction with various methods.*

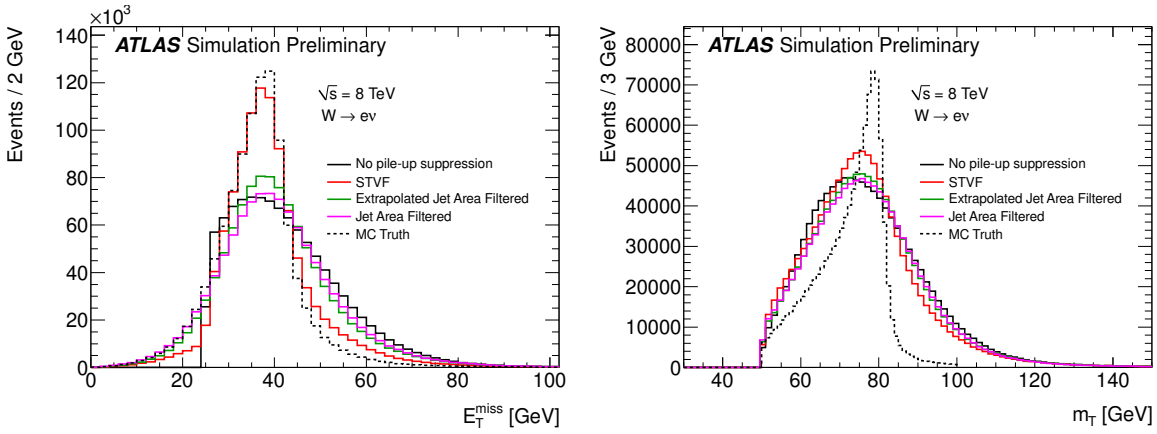

(a) (b)

Figure 27: *E_T^{miss} (a) and m_T (b) before and after pile-up suppression with different methods in all selected MC $W \to e\nu$ events. The true E_T^{miss} and the reconstructed m_T using the true $\boldsymbol{E}_T^{miss}$ are also shown for comparison.*

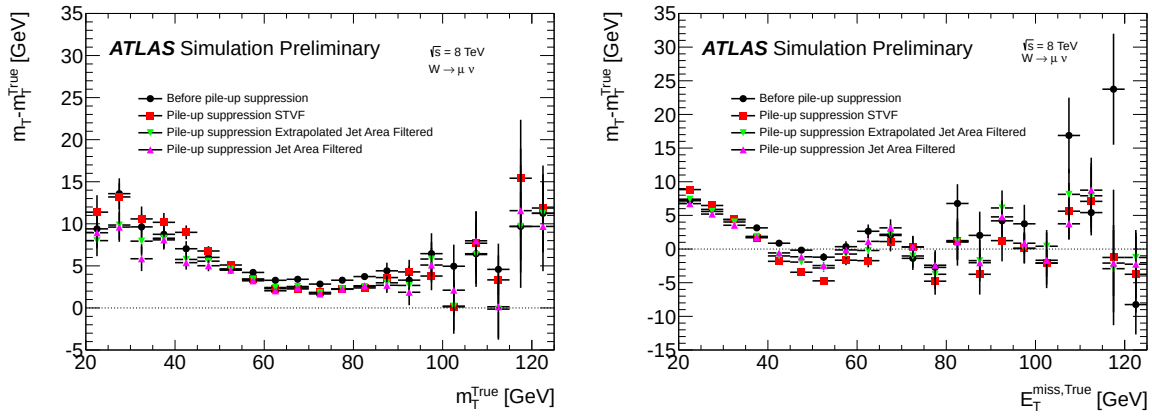

(a) (b)

Figure 28: $m_T - m_T{}^{True}$ *as a function of* $m_T{}^{True}$ *(a) and* $m_T - m_T{}^{True}$ *as a function of* $E_T^{miss,True}$ *(b) in* $W \to \mu\nu$ *events.*

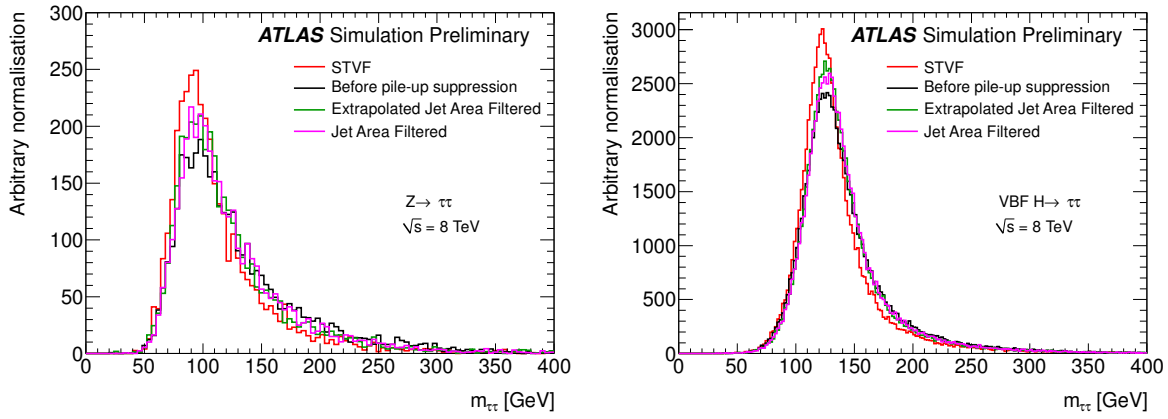

(a) (b)

Figure 29: *The reconstructed invariant* $m_{\tau\tau}$*, using the collinear approximation, in* $Z \to \tau\tau$ *(a) and in VBF* $H \to \tau\tau$ *(*$m_H = 125\,GeV$*) events (b) before and after pile-up suppression with different methods in MC simulation.*

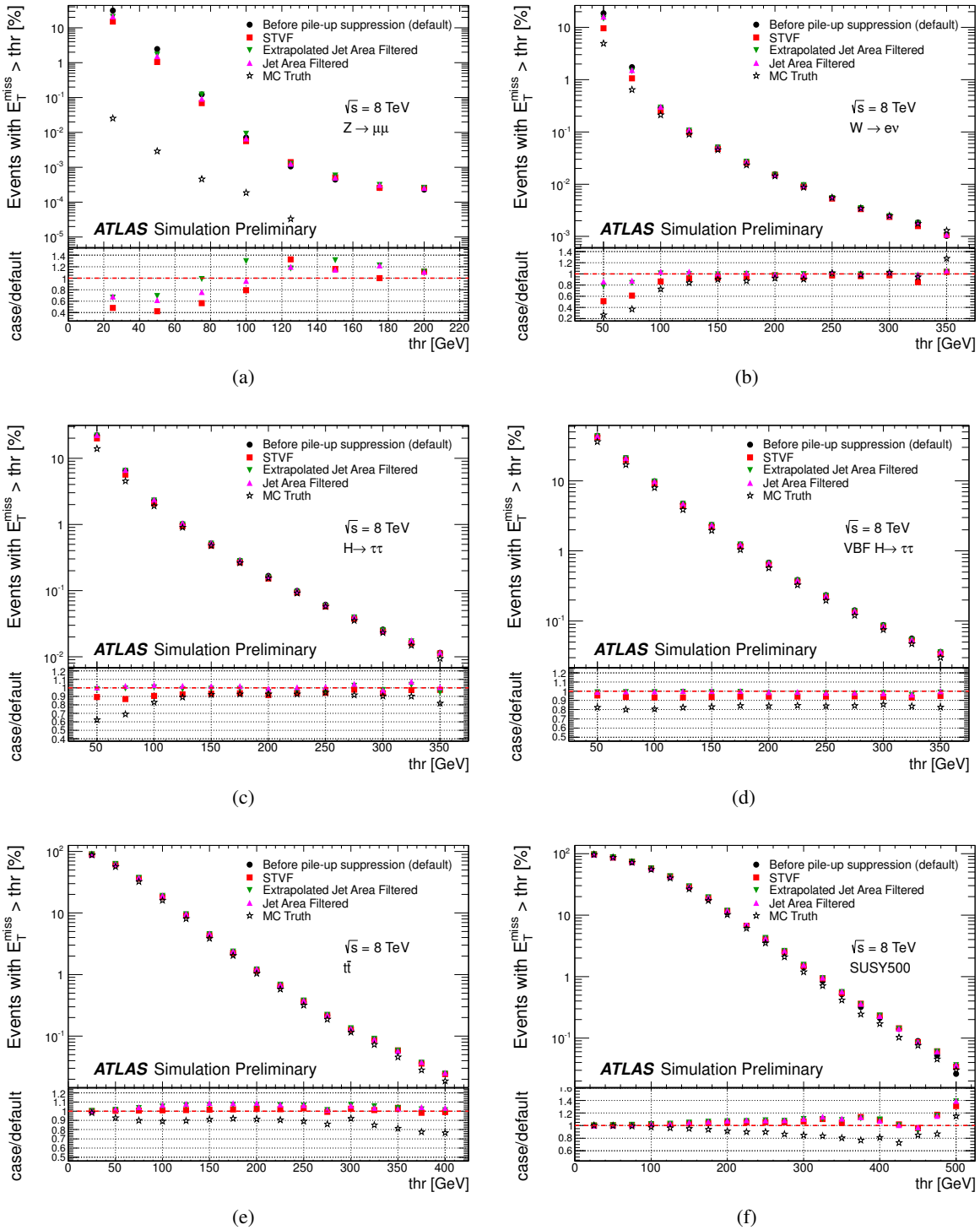

Figure 30: *Number of events with E_T^{miss} above a threshold in MC $Z \to \mu\mu$ (a), $W \to e\nu$ (b), $H \to \tau\tau$ (c), VBF $H \to \tau\tau$ (d), $t\bar{t}$ (e) and SUSY events (f) before and after pile-up suppression with different methods. The number of events with the true E_T^{miss} above threshold is also shown for comparison. The lower parts of the figures show the ratio of each case (pile-up suppression method or Truth) over the default (before pile-up suppression).*

$E_{\mathrm{T}}^{\mathrm{miss,SoftTerm}}$ uncertainty	data/MC method		balance method		
	scale	resolution	scale		resolution
	(%)	(%)	([GeV])	(%)	(%)
Default	3.6	2.3	< 1 GeV	<13	2.0
STVF	7.9	4.8	< 1 GeV	<12	4.5
Extrapolated Jet Area Filtered	4.7	2.0	< 1 GeV	< 18	3.0
Jet Area Filtered	5.8	2.5	< 1 GeV	< 16	2.0

Table 1: Systematic uncertainties on the scale and on the resolution of the $E_{\mathrm{T}}^{\mathrm{miss,SoftTerm}}$, calculated with the two different methods described in this section, the data/MC ratio described in 8.1 and the balance method described in 8.2. The scale variations reported in column 4 are observed at small values of $E_{\mathrm{T}}^{\mathrm{miss,SoftTerm}}$ and $p_{\mathrm{T}}^{\mathrm{hard}}$ (O (1 GeV)).

and the soft term. Before pile-up suppression the soft term is largely dominant with respect to the muon contribution, so the data-MC discrepancy can be covered taking into account only the uncertainties on the scale and the resolution of the soft term. Figure 31 shows that the data-MC ratios obtained scaling the soft term up and down according to its scale uncertainty and smearing it according to its resolution uncertainty can cover the deviation of data-MC ratio from unity in the full range. In STVF, although the uncertainties are larger with respect to the $\boldsymbol{E}_{\mathrm{T}}^{\mathrm{miss}}$ before pile-up suppression, the impact on the $E_{\mathrm{T}}^{\mathrm{miss}}$ spectrum is much smaller, since the soft term is not the dominant one in this case and it has a reduced magnitude.

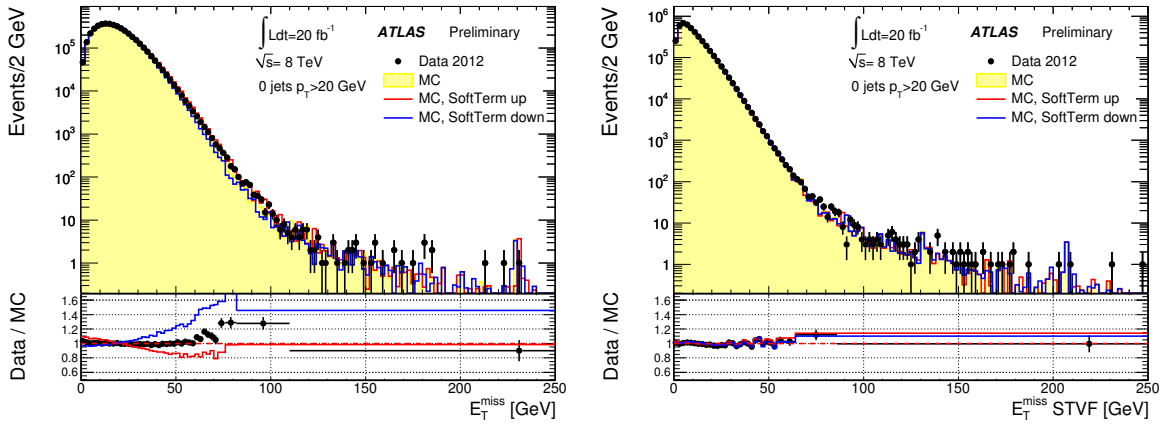

(a) (b)

Figure 31: *Distribution of $\boldsymbol{E}_T^{miss}$ before (a) and after pile-up suppression with STVF (b). Data are compared with the nominal $Z \rightarrow \mu\mu$ MC simulation and with the MC simulation calculated after scaling and smearing the $E_T^{miss,SoftTerm}$, according to the scale and resolution uncertainties calculated with the data/MC ratio method reported in Table 1. The lower parts of the figures show the ratio of data over MC, both for the nominal MC and MC calculated after scaling/smearing the soft term.*

Figure 32 shows the closure test for the systematic uncertainties, calculated with the balance method, in $Z \rightarrow \mu\mu$ events without jets. The results are similar to those shown in Figure 31 for the data/MC method. The uncertainties on the scale and the longitudinal and perpendicular resolution of the soft term can cover the data-MC discrepancy for the $E_{\mathrm{T}}^{\mathrm{miss,SoftTerm}}$ distribution, both before pile-up suppression and after pile-up suppression with STVF. When considering the total $E_{\mathrm{T}}^{\mathrm{miss}}$ distribution, the effect of

the uncertainties on the soft term is important before pile-up suppression and is almost negligible after STVF.

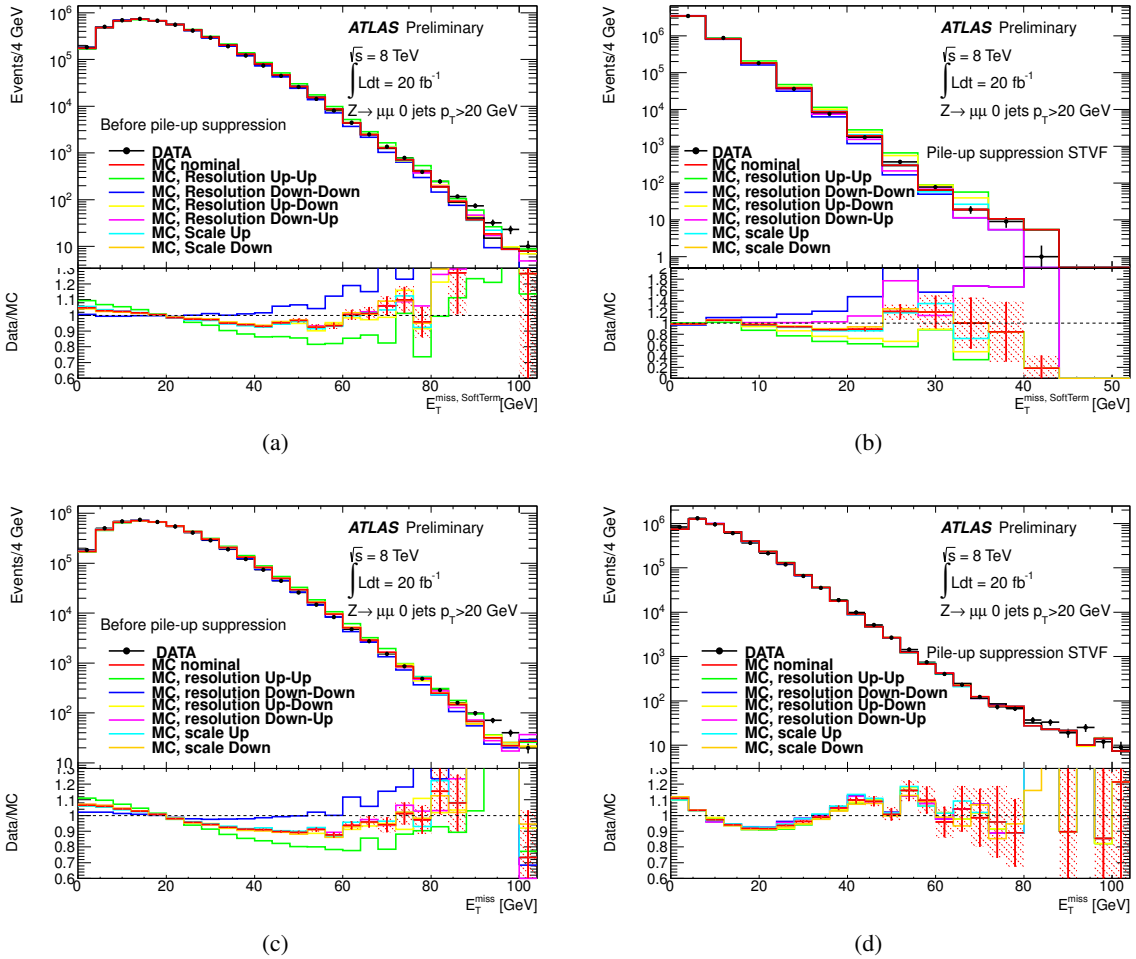

Figure 32: *Distributions of $E_T^{miss,SoftTerm}$ before (a) and after pile-up suppression with STVF (b) and of E_T^{miss} before (c) and after pile-up suppression with STVF (d). Data are compared with the nominal $Z \rightarrow \mu\mu$ MC simulation and with the MC simulation calculated after scaling/smearing the $E_T^{miss,SoftTerm}$ [2], according to the scale and resolution, both longitudinal and perpendicular, uncertainties calculated with the balance method reported in Table 1 . The lower parts of the figures show the ratio of data over MC, both for the nominal MC and MC calculated after scaling/smearing the soft term.*

9 Conclusions

The missing transverse momentum ($\boldsymbol{E}_{\mathrm{T}}^{\mathrm{miss}}$) performance has been studied in events with different topologies with and without genuine $\boldsymbol{E}_{\mathrm{T}}^{\mathrm{miss}}$ in proton-proton collisions at a centre-of-mass energy of 8 TeV recorded with the ATLAS detector in 2012.

The value of $\boldsymbol{E}_{\mathrm{T}}^{\mathrm{miss}}$ is calculated from calibrated reconstructed objects and from the unmatched topological clusters and tracks ($E_{\mathrm{T}}^{\mathrm{miss,SoftTerm}}$). Several methods for pile-up suppression in the soft term are described, based on the use of tracks (STVF method) or on the jet area method.

The Monte Carlo simulation describes the data in general rather well. Some differences are observed between data and MC simulation for the reconstructed total transverse energy, which is not well described by the POWHEG + PYTHIA8 Monte Carlo. A better description of the reconstructed total transverse energy is given by the ALPGEN Monte Carlo. Some additional discrepancy in data-MC comparison is observed after pile-up suppression in the $E_{\mathrm{T}}^{\mathrm{miss,SoftTerm}}$ and in the contribution from jets, due to the corrections applied for pile-up suppression.

The $\boldsymbol{E}_{\mathrm{T}}^{\mathrm{miss}}$ resolution improves after pile-up suppression in events where the contribution of the soft term is important and it becomes closer to that observed in the absence of pile-up, mainly with the STVF method.

The $\boldsymbol{E}_{\mathrm{T}}^{\mathrm{miss}}$ projected along the Z direction in $Z \to \ell\ell$ events, which is a measure of the $\boldsymbol{E}_{\mathrm{T}}^{\mathrm{miss}}$ scale, is in good agreement in data and MC simulation, but it is observed to have some bias, which increases after pile-up suppression especially with the STVF method. There is some difference in the observed bias between $Z \to \mu\mu$ and $Z \to ee$ events.

The linearity of the $\boldsymbol{E}_{\mathrm{T}}^{\mathrm{miss}}$ measurement in events with genuine $E_{\mathrm{T}}^{\mathrm{miss}}$ is studied in MC simulation as a function of the true $E_{\mathrm{T}}^{\mathrm{miss}}$. Except for the bias observed at small true $E_{\mathrm{T}}^{\mathrm{miss}}$ values (visible up to 40 GeV), due to the finite $\boldsymbol{E}_{\mathrm{T}}^{\mathrm{miss}}$ resolution, the linearity is better than 5% in all samples (apart from the STVF $\boldsymbol{E}_{\mathrm{T}}^{\mathrm{miss}}$in $W \to \ell\nu$ events) and it is very good in events with a very large number of jets, such as simulated SUSY events.

The systematic uncertainty on the scale and the resolution of the $\boldsymbol{E}_{\mathrm{T}}^{\mathrm{miss,SoftTerm}}$ is determined comparing data and MC $Z \to \ell\ell$ events with two different methods, and it is found to be of the order of a few percent. The effect of the uncertainty on the $\boldsymbol{E}_{\mathrm{T}}^{\mathrm{miss,SoftTerm}}$ has a visible effect on the $\boldsymbol{E}_{\mathrm{T}}^{\mathrm{miss}}$ only before pile-up suppression, while it is negligible after the pile-up suppression because of the strong reduction of the $E_{\mathrm{T}}^{\mathrm{miss,SoftTerm}}$.

References

[1] ATLAS Collaboration, *Performance of missing transverse momentum reconstruction in proton-proton collisions at 7 TeV in ATLAS*, Eur. Phys. J. C **72** (2012) 1844, arXiv:1108.5602.

[2] ATLAS Collaboration, *Performance of Missing Transverse Momentum Reconstruction in ATLAS with 2011 Proton-Proton Collisions at* $\sqrt{s} = 7$ *TeV*, ATLAS-CONF-2012-101.

[3] ATLAS Collaboration, *The ATLAS Experiment at the CERN Large Hadron Collider*, JINST **3** (2008) S08003.

[4] ATLAS Collaboration, *Data-Quality Requirements and Event Cleaning for Jets and Missing Transverse Energy Reconstruction with the ATLAS Detector in Proton-Proton Collisions at a Center of Mass Energy* $\sqrt{s} = 7$ *TeV*, ATLAS-CONF-2010-038.

[5] ATLAS Collaboration, *Luminosity Determination in pp Collisions at 7 TeV using the ATLAS Detector at the LHC*, Eur. Phys. J. C **071** (2011) 1630, arXiv:1101.2185.

[6] ATLAS Collaboration, *Luminosity Determination in pp Collisions at* $\sqrt{s} = 7$ *TeV using the ATLAS Detector in 2011*, ATLAS-CONF-2011-116.

[7] ATLAS Collaboration, *Charged-particle multiplicities in pp interactions measured with the ATLAS detector at the LHC*, New J. Phys. **13** (2011) 053033.

[8] ATLAS Collaboration, *Muon Reconstruction Performance*, ATLAS-CONF-2010-064.

[9] ATLAS Collaboration, *Measurement of the* $W \to l\nu$ *and* $Z \to ll$ *production cross sections in proton-proton collisions at* $\sqrt{s} = 7$ *TeV with the ATLAS detector*, JHEP **12** (2010) 060, arXiv:1010.2130.

[10] ATLAS Collaboration, *Electron performance measurements with the ATLAS detector using the 2010 LHC proton-proton collision data*, Eur. Phys. J. C **72** (2012) 1909, arXiv:1110.3174.

[11] P. Nason, *A New method for combining NLO QCD with shower Monte Carlo algorithms*, JHEP **0411** (2004) 040, arXiv:0409146.

[12] T. Sjostrand, S. Mrenna, and P. Z. Skands, *A Brief Introduction to PYTHIA 8.1*, Comput. Phys. Commun. **178** (2008) 852–867, arXiv:0710.3820 [hep-ph].

[13] R. Corke and T. Sjostrand, *Interleaved Parton Showers and Tuning Prospects*, JHEP **032** (2011) 1103, arXiv:1011.1759.

[14] H. Lai et al., *New parton distributions for collider physics*, Phys. Rev. **D82** (2010) , arXiv:1007.2241.

[15] ATLAS Collaboration, *Summary of ATLAS Pythia 8 tunes*, ATL-PHYS-PUB-2012-003.

[16] M. L. Mangano, M. Moretti, F. Piccinini, R. Pittau, and A. D. Polosa, *ALPGEN, a generator for hard multiparton processes in hadronic collisions*, JHEP **07** (2003) 001, arXiv:0206293 [hep-ph].

[17] S. Frixione and B. R. Webber, *Matching NLO QCD computations and parton shower simulations*, JHEP **06** (2002) 029.

[18] M. Bahr et al., *Herwig++ physics and manual*, Eur. Phys. J. **C 58** (2008) 639–707, arXiv:0803.0883 [hep-ph].

[19] A. Martin et al., *Parton distributions for the LHC*, Eur. Phys. J. **C63** (2009) , arXiv:0901.0002.

[20] GEANT4 Collaboration, S. Agostinelli et al., *GEANT4: A simulation toolkit*, Nucl. Instrum. Meth. **A 506** (2003) 250–303.

[21] ATLAS Collaboration, *The ATLAS simulation infrastructure*, Eur. Phys. J. **C 70** (2010) 823–874, arXiv:1005.4568 [physics.ins-det].

[22] W. Lampl et al., *Calorimeter clustering algorithms: Description and performance*, ATL-LARG-PUB-2008-002.

[23] T. Barillari et al., *Local Hadronic Calibration*, ATL-LARG-PUB-2009-001.

[24] ATLAS Collaboration, *Jet energy measurement with the ATLAS detector in proton-proton collisions at 7 TeV*, submitted to Eur. Phys. J. C , arXiv:1108.5602.

[25] ATLAS Collaboration, *Determination of the tau energy scale and the associated systematic uncertainty in proton-proton collisions at* $\sqrt{(s)} = 7$ *TeV with the ATLAS detector at the LHC in 2011*, ATLAS-CONF-2012-054.

[26] M. Cacciari, G. P. Salam, and G. Soyez, *The anti-k_t jet clustering algorithm*, JHEP **05** (2008) 063, arXiv:0802.1189.

[27] M. Cacciari, G. P. Salam, and G. Soyez, *The Catchment Area of Jets*, JHEP **0804** (2008) 005, arXiv:0802.1188 [hep-ph].

[28] S. Catani, Y. L. Dokshitzer, M. Seymour, and B. Webber, *Longitudinally invariant K_t clustering algorithms for hadron hadron collisions*, Nucl.Phys. **B406** (1993) 187–224.

[29] S. D. Ellis and D. E. Soper, *Successive combination jet algorithm for hadron collisions*, Phys.Rev. **D48** (1993) 3160–3166, arXiv:hep-ph/9305266 [hep-ph].

[30] ATLAS Collaboration, *Expected performance of the ATLAS experiment - detector, trigger and physics (Jet and E_T^{miss} chapter)*, tech. rep., 2009. arXiv:0901.0512 [hep-ex]. CERN-OPEN-2008-020.

[31] ATLAS Collaboration, *Search for the Standard Model Higgs boson in the H to tau-tau decay mode in 7 TeV pp collisions with ATLAS*, JHEP **09** (2012) 070.